Therefore, to test the aforementioned hypothesis, we explored the effect of PDE3 inhibition both on platelet aggregation induced by ristocetin, a non-physiological inducer of VWF binding to GPIbα and on platelet thrombus formation on a VWF or collagen surface under flow conditions at wall shear rates of 150 s^{-1} (low shear) or 1,500 s^{-1} (high shear) by utilising parallel plate flow chambers *in vitro*. Cilostazol is not appropriate for *in vitro* experiments to deduce its clinical effect because its active metabolites also play major roles in its pharmacological effects on human (12). Cilostazol neither increases cAMP levels of human platelets nor inhibits shear stress-induced platelet aggregation at therapeutic concentration in the absence of Gs stimulator *in vitro* (13). Moreover, the specificity of cilostazol is less selective for PDE3 isozyme (14). Hence, to specifically evaluate the effect of PDE3 inhibition on platelet function *in vitro*, we used a more potent and selective PDE3 inhibitor, K-134 (6-(3-(3-cyclopropyl-3-(2-hydroxycyclohexyl)ureido)propoxy)-2(1H)-quinolinone, also known as OPC-33509), which is a cilostazol analogue but is not a pro-drug (14, 15). While IC_{50} of cilostazol towards PDE2, PDE3A and PDE5 are 45.2, 0.20 and 4.4 μM, respectively, those of K-134 are >300, 0.10 and 12.1 μM, respectively (14). Here, we demonstrated that the K-134 effectively suppressed *in vitro* platelet thrombus formation under flow conditions in a more shear-dependent manner than ASA or the GPIIb/IIIa inhibitor tirofiban, and the effect of K-134 was apparent only in the presence of a low concentration of the AC stimulator PGE1. We propose that our data indicate a mechanism whereby PDE3 inhibition exhibits efficient antiplatelet effects on arterial thrombosis with a minimal impact on primary haemostasis.

Materials and methods

Antiplatelet reagents

The PDE3 inhibitors K-134 and cilostazol were obtained from Kowa (Tokyo, Japan). The GPIIb/IIIa inhibitor tirofiban was purchased from Toronto Research Chemicals (Toronto, Canada). The cyclooxygenase inhibitor ASA, Arg-Gly-Asp-Ser (RGDS) peptides (inhibitors of integrins with RGD binding sites), and forskolin (an AC activator) were from Sigma-Aldrich (St Louis, MO, USA). These reagents were dissolved in dimethyl sulfoxide (DMSO). PGE1 was purchased from Cayman Chemical (Ann Arbor, MI, USA) and dissolved in ethanol (EtOH). An inhibitory mouse monoclonal antibody against human GPIbα, GUR83–35, was obtained from Takara Bio (Shiga, Japan), and the isotype-matched control mouse IgG1 was purchased from SIGMA-Aldrich. The selection of K-134 concentrations is based on the phase-I study and non-clinical study, in which K-134 treatment with a maximal serum concentration of 1–5 μM showed antiplatelet effects on human *ex vivo* and beneficial effects in a rat model of thrombosis or ischaemia (manuscript in preparation).

Blood sampling

After obtaining informed consent according to the Declaration of Helsinki, blood was collected from the antecubital vein of healthy, medication-free volunteers through a 21-gauge needle and was anticoagulated with D-phenylalanyl-L-prolyl-L-arginine chloromethyl ketone dihydrochloride (PPACK; Calbiochem, San Diego, CA, USA) (final concentration (fc), 40 μM) or a 10% volume of 3.8% (w/v) sodium citrate. Platelet-rich plasma (PRP) was prepared by centrifugation (100 *g*, 15 minutes [min], 22°C) of blood, and the platelet count was adjusted to 2.0×10^5/μl with platelet-poor plasma prepared by centrifugation (2,200 *g*, 10 min, 22°C) for agonist-induced platelet aggregation assay. The platelet concentration was determined using an automated haematology analyzer (K-4500; Sysmex, Kobe, Japan).

Agonist-induced platelet aggregation

PPACK-anticoagulated PRP was incubated with antiplatelet agents with or without 6 nM PGE1 at 37°C for 2 min and stimulated with adenosine diphosphate (ADP) (fc, 10 μM; MC Medical, Tokyo, Japan) or collagen (fc, 1.75–2.75 μg/ml; Chronolog, Havertown, PA, USA). ADP- or collagen-induced platelet aggregation was quantified by measuring maximum aggregation rate (MAR; percent of maximal light transmittance) within 5 min after addition of trigger using an aggregometer (Hema Tracer T-638; Nico Bioscience, Tokyo, Japan) (n=3). All volunteers' PRP samples showed similar dose-response curves for ADP (EC_{50}: about 5 μM, MAR induced by 10 μM ADP: 55–65%). The concentration of collagen was adjusted to give the EC_{85}. Ristocetin-induced platelet aggregation (RIPA) was performed by adding ristocetin solution (fc, 1.5 mg/ml; Sigma-Aldrich) to citrated PRP after incubation with antiplatelet agents at 37°C for 5 min. The effects of antiplatelet agents on RIPA were evaluated by aggregation rates at 10 min after addition of trigger. All volunteers' PRP samples (n=4) showed similar dose-response curves for ristocetin (EC_{50}: about 1.2 mg/ml, aggregation rate at 10 min: > 90%).

Preparation of thrombogenic substrate-coated surfaces

Human VWF (10 μg/ml; purified from plasma as previously described [16]) and type I collagen derived from porcine tendon (30 μg/ml; Cellmatrix Type I-A, Nitta Gelatin, Osaka, Japan) were prepared in Dulbecco's phosphate-buffered saline (PBS). Glass coverslips (No. 5, diameter 24 mm, thickness 0.5 mm; Matsunami Glass, Osaka, Japan) were immersed in VWF (22°C, 2.5 h) or collagen (4°C, 12 h) solution, carefully rinsed with PBS, and then blocked with bovine serum albumin (20 mg/ml; Sigma-Aldrich) in PBS (22°C, >2 h). After additional rinsing with PBS, coverslips were assembled into a parallel plate flow chamber just before perfusion experiments.

Perfusion experiments

PPACK-anticoagulated whole blood (5 ml) was incubated with a fluorescent marker ($DiOC_6$; Molecular Probes, Eugene, OR, USA) and antiplatelet agents at 37°C for 5 min, then aspirated using a roller pump (Minipulse 3; Gilson, Villiers Le Bel, France) and perfused over thrombogenic substrate-coated glass coverslips at a wall shear rate of 150 or 1,500 s^{-1} in a recirculating chamber (circulation cycle, 180 s or 18 s, respectively) mounted on an inverted epifluorescence microscope (Eclipse TE300; Nikon, Tokyo, Japan) equipped with a charge-coupled device camera (C2400–80V; Hamamatsu Photonics, Hamamatsu, Japan). These experiments were performed at 37°C and recorded on S-VHS videotape using a video cassette recorder (BR-S662; Victor, Tokyo, Japan), and digital images were captured using an Argus-50 image processor (Hamamatsu Photonics) with fixed contrast and brightness. The percentage of total area covered with platelets (designated as surface coverage) and the mean size of surface-bound platelet aggregates (designated as average platelet aggregate size) were calculated using the Argus-50 software. Surface coverage reflects platelet adhesion to the thrombogenic substrate-coated surface (2-dimensional thrombus growth), while average platelet aggregate size represents the degree of platelet aggregation (3-dimensional thrombus growth) on the surface (17, 18). We chose threshold values (grayness level from 0–255, where 0 is black) of 50 for surface coverage and 200 for average platelet aggregate size, to eliminate background fluorescence and fluorescence of single platelets that do not aggregate, respectively.

Measurement of cAMP and cGMP

Citrated PRP was pre-incubated with K-134 with or without 6 nM PGE1 at 37°C for 5 min, and simulated with ristocetin (fc, 1.5 mg/ml) for 10 min under stirring. Platelet intracellular cAMP and cGMP levels were analysed using an Amersham cAMP/cGMP Biotrak Enzymeimmunoassay system (GE Healthcare, Buckinghamshire, UK) and were presented as a concentration of cAMP or cGMP pmol/10^8 platelets.

Statistical analysis

Statistical analyses were performed using SAS Preclinical Package version 5.0 software (SAS Institute Japan, Tokyo, Japan).

Results

Effects of PDE3 inhibitors on RIPA

First, we compared the inhibitory effects of the PDE3 inhibitors cilostazol and K-134 with other antiplatelet agents on RIPA *in vitro*.

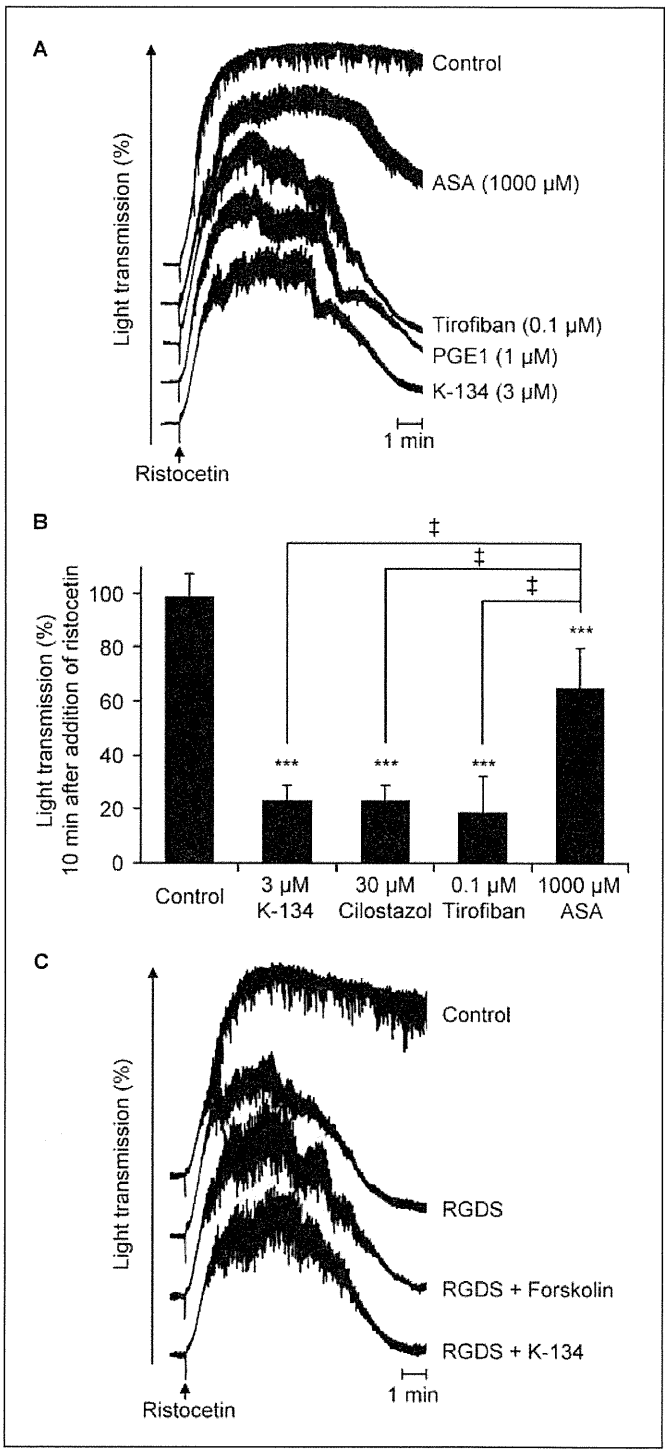

Figure 1: Effects on ristocetin-induced human platelet aggregation. Citrated PRP was preincubated with DMSO (control) or each antiplatelet agent, and stimulated with ristocetin. A, B) Inhibitory effects of agents were estimated by measuring platelet aggregation rate (%) at 10 min after stimulation (n=5). ***p<0.001 vs. control, ‡p<0.001 vs. ASA group (Tukey's test). C) The effects of 10 μM forskolin and 10 μM K-134 on ristocetin-induced platelet agglutination were evaluated in the presence of 1 μM RGDS peptides. The agglutination and aggregation curves are representatives of five experiments. Values are mean ± SD.

IC50 (μM)	Ristocetin	Ristocetin (+PGE1)	ADP	ADP (+PGE1)	Collagen	Collagen (+PGE1)
K-134	2.2 (2.0–2.4)	0.77 (0.47–1.1)	6.1 (4.4–8.3)	0.95 (0.76–1.2)	0.74 (0.55–1.0)	0.24 (0.18–0.33)
Cilostazol	22 (18–25)	8.3 (4.8–12)	32 (24–42)	7.3 (6.5–8.2)	6.4 (5.5–7.5)	1.6 (1.4–1.8)
Tirofiban	0.045 (0.011–0.072)	0.061 (0.049–0.072)	0.028 (0.018–0.042)	0.027 (0.021–0.034)	0.022 (0.019–0.026)	0.016 (0.012–0.022)
ASA	>1000	>1000	>1000	>1000	59 (39–91)	55 (40–73)

Table 1: Effects of PDE3 inhibitors on ristocetin-, ADP- or collagen-induced platelet aggregation. Calculated half-maximal inhibitory concentration (IC_{50}) values are expressed as the mean from 3–4 human volunteers. Values in parentheses indicate 95% confidence intervals.

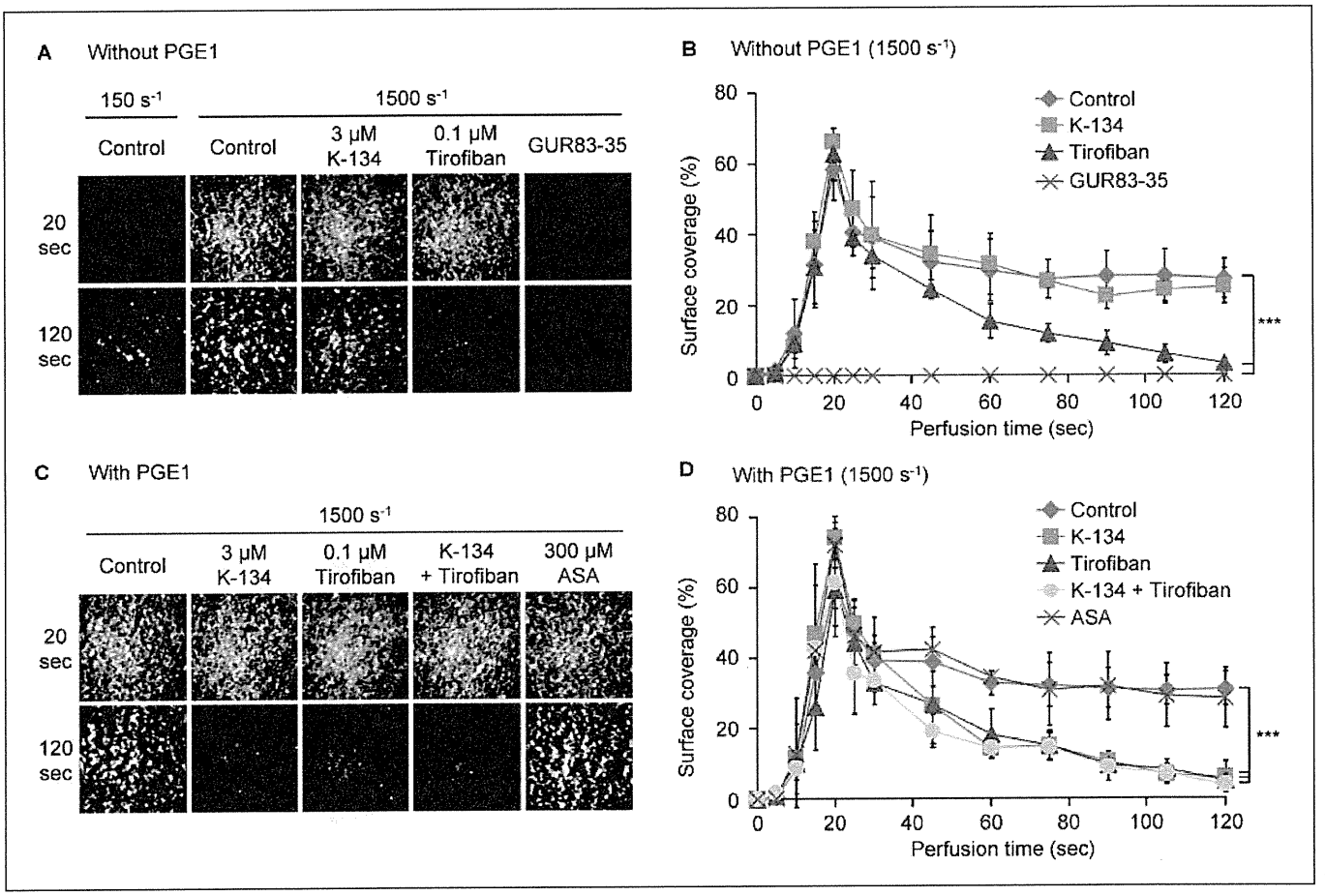

Figure 2: Effects on thrombus formation on a VWF surface under flow. PACK-anticoagulated blood was incubated with DiOC6 for platelet visualisation and DMSO (control) or each antiplatelet agent, and perfused over VWF-immobilised glass coverslips in a parallel plate flow chamber at a wall shear rate of 150 s^{-1} (A) or 1,500 s^{-1} (A-D) in the absence (A, B) or presence (C, D) of 6 nM PGE1. To confirm the GPIbα-dependency of platelet binding to VWF, 15 μg/ml GUR83–35 was used as a GPIbα blocking antibody. The effect of each inhibitor on platelet initial accumulation via GPIbα and on subsequent platelet aggregation was evaluated by measuring surface coverage at 0–120 s after initiation of perfusion. A, C) Representative images, corresponding to a 220 × 220 μm area at 20 or 120 s after initiation of perfusion. ***p<0.001 vs. control (Tukey's test was performed at 120 s). Values are mean ± SD (n=6 for control and n=3 for others).

In effect, 3 μM K-134 and 30 μM cilostazol significantly (p<0.001) inhibited RIPA (evaluated at 10 min after addition of trigger) to the same extent as 0.1 μM tirofiban and 1 μM PGE1, and more potently than 1,000 μM ASA (▶Fig. 1A, B). To explore the effects of PDE3 inhibitor on GPIIb/IIIa-independent platelet agglutination mediated through direct interaction between VWF and GPIb/V/IX, PRP was incubated with an integrin-antagonist peptide, RGDS, before ristocetin stimulation. Under such conditions, K-134 caused no change in agglutination extent and the same was true with PGE1 (not shown) and forskolin, which also increases in-

tracellular cAMP levels via direct AC activation (▶Fig. 1C). It was found that GUR83–35, a monoclonal antibody against GPIbα completely suppressed the agglutination phenomenon (not shown). These results indicate that an intracellular cAMP level heightened by PDE3 inhibition or AC activation is a crucial down-regulator for platelet aggregation via VWF-GPIb/V/IX-mediated signals, but not for VWF-GPIb/V/IX interaction itself that is independent of GPIIb/IIIa.

Next, we examined the synergistic effects of concomitant stimulation of AC on the observed PDE3 inhibition of RIPA. Inducible Gs-coupled receptor stimulation by vascular wall-derived PGI2 or adenosine is thought to be pathologically relevant in the circulation to defend against thrombosis (19, 20). Therefore, to mimic the *in vivo* situation *in vitro*, we conducted aggregation study in the presence of a very low concentration (6 nM) of PGE1. Our preliminary experiments demonstrated that 6 nM PGE1 was close to the optimal concentration that could elevate cAMP levels in the presence of PDE3 inhibitor, but did not affect agonist-induced platelet aggregation in the absence of PDE3 inhibitor (not shown). Indeed, the inhibitory effects of PDE3 inhibitors on not only ADP- or collagen- but also ristocetin-induced platelet aggregation were readily augmented in the presence of 6 nM PGE1 (▶Table 1). In contrast, the effects of tirofiban and ASA were unaffected by PGE1. Taken together, these results indicate that similar to other signals stimulated by ADP and collagen under stirring conditions, the GPIb/V/IX signal elicited by VWF binding is a cAMP-sensitive pathway.

PDE3 inhibition prevents stable platelet thrombus formation on a VWF surface under flow

To further clarify the effect of PDE3 inhibition on VWF-GPIb/V/IX-mediated platelet activation under physiological conditions, PPACK-anticoagulated blood was perfused over VWF coated onto glass coverslips. Under arterial flow conditions at a high wall shear rate of 1,500 s^{-1}, platelets exhibited rapid and progressive attachment onto the VWF surface with a peak surface coverage of ~70% at 20 s after perfusion (▶Fig. 2A, B). Platelets then started to detach over time (possibly due to the unstable platelet adherence induced by recirculating small platelet aggregates), and stable thrombus formation (surface coverage ~30%) was finally constructed by 120 s. In contrast, at a venous wall shear rate of 150 s^{-1}, platelet thrombus tended to grow slowly on the VWF surface with surface coverage of about 10% even at 120 s (▶Fig. 2A), and was not completely abolished by the previous addition of GUR83–35 (not shown). The effect of K-134 on platelet thrombus formation was studied under arterial flow conditions (1,500 s^{-1}). Unexpectedly, K-134 at a therapeutic concentration of 3 μM did not affect the whole profile of thrombus formation, while tirofiban showed an apparent inhibitory effect on the second phase of thrombus formation (at 20–120 s). Although tirofiban did not affect the first phase of platelet contact at 0–20 s, GUR83–35 completely blocked this platelet interaction (▶Fig. 2A, B) but the isotype-matched control mouse IgG1 did not show any effect (not shown), indicating that the first phase of the interaction involves GPIIb/IIIa-independent initial contact of platelets onto VWF via GPIb/V/IX (▶Fig. 2A, B). Prominently enough, although 6 nM PGE1 itself had no inhibitory effect on platelet thrombus formation at such low concentration, K-134 showed a potent inhibitory effect on the second phase of platelet interaction in the presence of 6 nM PGE1 (▶Fig. 2C, D). The extent of inhibition by K-134 resembled that by tirofiban and no synergic effect from both inhibitors was observed. In contrast, ASA showed no inhibitory effect under these experimental conditions. These results of perfusion experiments thus indicate that under physiological flow conditions, antiplatelet effects by PDE3 inhibition are mediated by elevated cAMP to efficiently block the initial signalling of the VWF-GPIb/V/IX pathway and subsequent autocrine activation signals, and the inhibitory effect is only significant in the presence of concomitant low level stimulation of AC.

PDE3 inhibition suppresses platelet thrombus formation on a collagen surface in a shear-dependent manner

To evaluate the effect of PDE3 inhibition on platelet thrombus formation mediated simultaneously by both collagen and VWF, we performed perfusion experiments over glass coverslips coated with type I collagen fibrils, to which plasma-derived VWF was expected to adsorb via the A3 domain. Indeed, we observed that platelet thrombus formation on the collagen surface under high shear (1,500 s^{-1}) was completely blocked by anti-GPIbα antibody

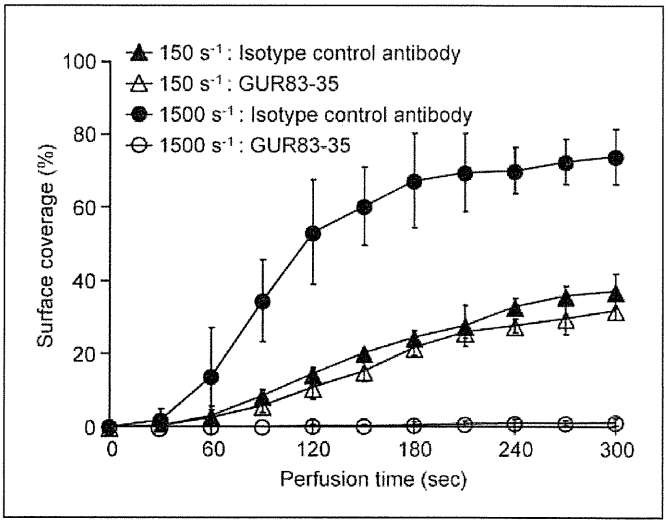

Figure 3: Effect of GPIbα blocking on thrombus formation on a collagen surface under flow. Blood treated as described in the legend for Figure 2 was perfused over collagen-immobilised glass coverslips. Effects of GPIbα blocking antibody, GUR83–35 (15 μg/ml) on thrombus formation at a wall shear rate of 150 or 1,500 s^{-1} was evaluated by measuring surface coverage. Values are mean ± SD (n=3).

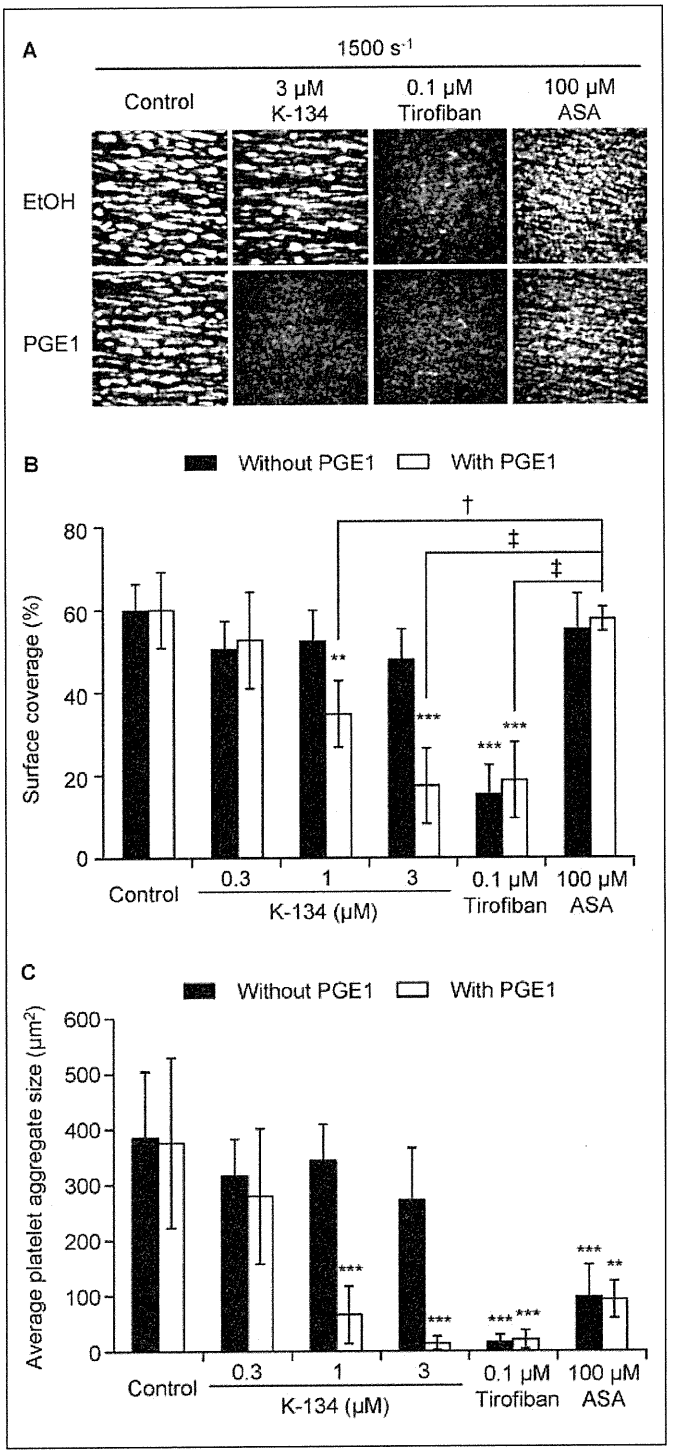

Figure 4: Effects on thrombus formation on a collagen surface under high shear. Blood treated as described in the legend for Figure 2 was perfused over collagen-immobilised glass coverslips at a wall shear rate of 1,500 s^{-1}. A) Representative images corresponding to a 340 x 340 μm area, captured at 270 s after initiation of perfusion. Effects on platelet adhesion and aggregation were evaluated by measuring surface coverage (B) and average platelet aggregate size (C), respectively. **p<0.01, ***p<0.001 vs. control. †p<0.05, ‡p<0.001 vs. ASA with PGE1 group (Tukey's test). Values are mean ± SD (n=8 for control, n=4 for others).

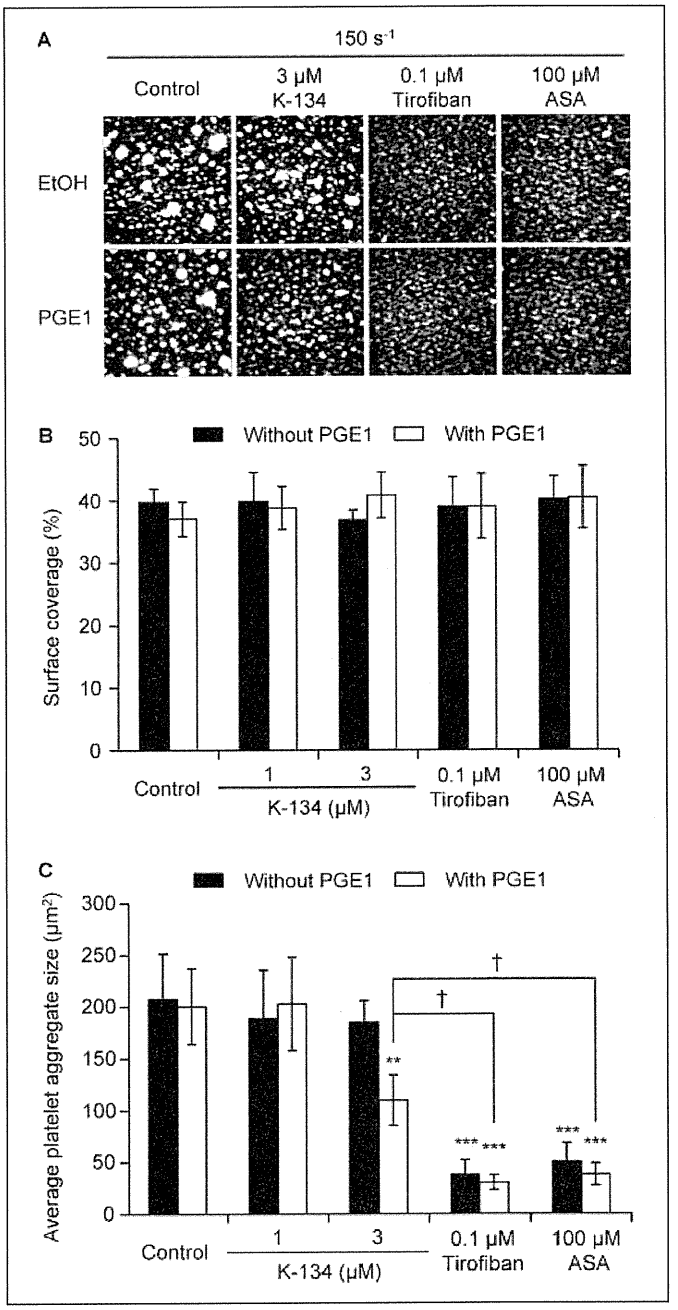

Figure 5: Effects on thrombus formation on a collagen surface under low shear. Blood treated as described in the legend for Figure 2 was perfused over collagen-immobilised glass coverslips at a wall shear rate of 150 s^{-1}. A) Figure shows representative images, corresponding to a 340 x 340 μm area, captured at 270 s after initiation of perfusion. Effects on platelet adhesion and aggregation were evaluated by measuring surface coverage (B) and average platelet aggregate size (C), respectively. **p<0.01, ***p<0.001 vs. control, †p<0.05 vs. 3 μM K-134 with PGE1 group (Tukey's test). Values are mean ± SD (n=4).

GUR83–35, while the antibody was without effect on thrombus formation under low shear (150 s^{-1}) (▶Fig. 3). Consistent with previous findings (8, 11), these results indicate that platelet adhesion and subsequent aggregation onto the collagen surface

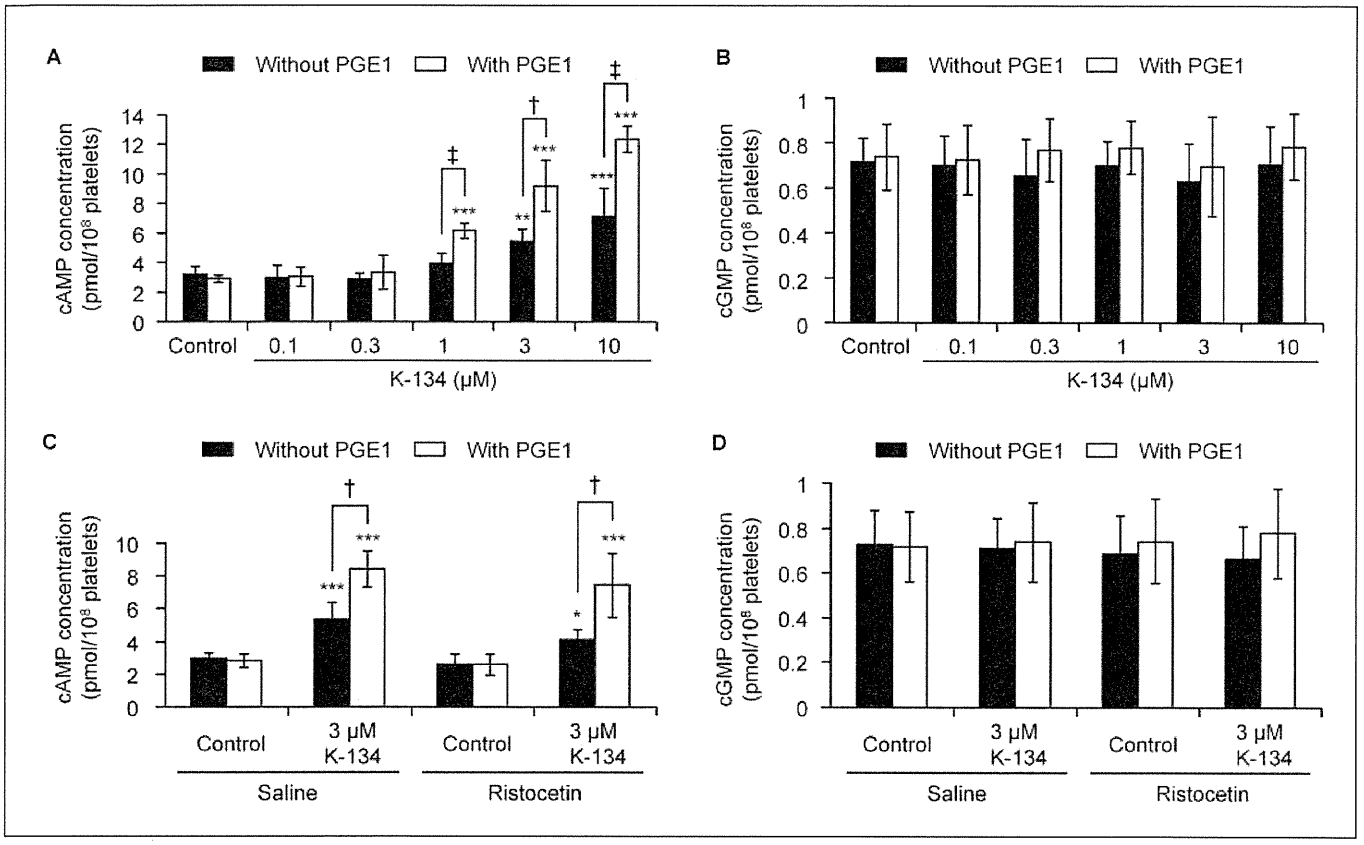

Figure 6: Effects on platelet cAMP and cGMP levels. Citrated PRP was pretreated with DMSO (control) or K-134 with or without 6 nM PGE1 for 5 min, and incubated with ristocetin or vehicle control (saline) for 10 min under stirring. A, B) platelet cAMP and cGMP levels after K-134 pretreatment (n=5). **p<0.01, ***p<0.001 vs. control (Dunnett's test), †p<0.01, ‡p<0.001 vs. absence of PGE1 (t-test). C, D) platelet cAMP and cGMP levels after ristocetin-stimulation (n=5). *p<0.05, ***p<0.001 vs. control (Tukey's test). Values are mean ± SD.

under flow conditions is mediated through VWF-GPIb/V/IX engagement in a shear rate-dependent manner. We then tested the effects of antiplatelet agents on platelet thrombus formation on the collagen surface under flow conditions. Under high shear, K-134 at least at a therapeutic concentration (~3 μM) was found to be inhibitory only when a low concentration of PGE1 (6 nM) was present (▶Fig. 4A). In fact, K-134 readily suppressed irreversible platelet adhesion (surface coverage at 270 s) and stable thrombus formation by platelet aggregation (average platelet aggregate size at 270 s) on the collagen surface in a dose-dependent manner in the presence of PGE1 (▶Fig. 4B, C). Conversely, tirofiban showed potent inhibitory effects on both parameters regardless of the presence or absence of PGE1, whereas ASA was without effects on surface coverage, but effectively (with a weaker effect than K-134 or tirofiban) inhibited platelet aggregate size. In contrast, under low shear, these antiplatelet agents including K-134 did not show any inhibitory effect on platelet surface coverage even in the presence of PGE1 (▶Fig. 5A, B). Of note, however, was the finding that these agents exhibited significant inhibitory effects on platelet aggregate size and the effect of K-134 became apparent only in the presence of PGE1 (▶Fig. 5A, C). Also, compared with results obtained under high shear (▶Fig. 4), the inhibitory effects of K-134 under low shear were significantly weaker than those of 0.1 μM tirofiban or 100 μM ASA ($p<0.05$).

Taken together, these results indicate that shear-dependent platelet thrombus formation *in vitro* initiated by GPIb/V/IX signalling is sensitive to cAMP-mediated regulatory pathways elicited by PDE3 inhibition in the presence of a low concentration of AC stimulator PGE1.

PDE3 inhibition increases platelet intracellular cAMP levels but not cGMP

To ascertain if the inhibitory effect of K-134 are mediated through cAMP or an alternative mechanism, we measured the intracellular cAMP and cGMP levels of platelets treated with K-134. Indeed, K-134 dose-dependently increased platelet cAMP levels but not cGMP, and the effect was potentiated by a low concentration of PGE1 (▶Fig. 6A, B). Furthermore, the cAMP-elevating effect of K-134 was also maintained in platelets activated by ristocetin under stirring conditions, while K-134 had no effect on cGMP levels (▶Fig. 6C, D).

Discussion

The GPIb/V/IX engagement with VWF immobilised on the subendothelial collagen surface under arterial flow conditions not only mediates platelet recruitment, but also initiates cellular activation leading to integrin-dependent firm platelet adhesion and aggregation at the site of vascular injury (8, 11). In fact, our findings (▶Figs. 1, 2) indicated that the observed suppression of VWF-mediated platelet thrombus formation by PDE3 inhibitors was due to efficient blocking of VWF-induced GPIb/V/IX signalling by elevated cAMP, but was not attributable to the down-regulation of GPIb/V/IX binding affinity with the ligand led by PKA-induced phosphorylation of the GPIbα subunit intracellular domain, which is contrary to previously reported study (21). Consistent with our finding, Mazzucato et al. (18, 22) reported that the magnitude of platelet translocation velocity on immobilised VWF in the presence of cAMP elevating reagents appeared to be the same as that obtained by GPIIb/IIIa blocking in similar perfusion experiments, while raising cAMP levels achieved complete inhibition of intracellular Ca^{2+} elevation and GPIIb/IIIa-mediated stable adhesion and aggregation.

PDE3 inhibitor reduced stable platelet thrombus formation on the collagen surface under high shear in the presence of PGE1 more potently than ASA, but had much lower inhibitory effects under low shear than tirofiban or ASA (▶Figs. 4, 5). There is a possible simple explanation as to why PDE3 inhibitor interfered with thrombus formation on the collagen surface in a more shear-dependent manner than tirofiban and ASA: while the secretion-independent signal mediated by VWF bound onto collagen is very sensitive to cAMP, that by collagen through GP VI is resistant to cAMP. In fact, PGE1, but not ADP receptor antagonists and ASA, could obliterate VWF-GPIb/V/IX-mediated initial intracytoplasmic Ca^{2+} oscillation (18). Moreover, cAMP analog strongly blocked GPIIb/IIIa activation induced by the dimeric VWF A1 domain (through GPIb/V/IX) in the presence of inhibitors of autocrine signalling through ADP and thromboxane A_2 (TXA_2) receptors (9). In addition, Shaun P. Jackson's group reported that platelet adhesion to VWF under high shear (at 600 and 1,800 s^{-1}) was not dependent on either ADP or TXA_2 (23). A primary collagen receptor of platelets is GPVI, which activates c-Src and Syk kinases leading to full cellular activation. In fact, tyrosine phosphorylation of these kinases induced by an anti-GPVI antibody or collagen was not abrogated with PGI2 treatment (24). Also, marked elevation of cAMP by forskolin reportedly did not inhibit collagen-induced and secretion-independent signalling events including protein-tyrosine phosphorylation, polyphosphoinositide liberation and granular secretion (25). In contrast, GP IV-mediated platelet aggregation (which is secretion-dependent) was completely inhibited by cAMP-elevating agents (24). Thus our findings were consistent with the fact that stable platelet thrombus formation on collagen under high shear is dependent on GPIb/V/IX signalling triggered by VWF and that under low shear that is mediated by GP VI signalling triggered by collagen itself (8, 10, 23).

Gs stimulation with PGE1 or adenosine and PDE3 inhibition synergistically accumulate cAMP to suppress platelet activation (1, 20). In fact, our results indicated that the observed antiplatelet effects of K-134 are most likely to be due to cAMP rather than to cGMP elevation (▶Fig. 6). Although K-134 alone potently inhibited VWF-dependent platelet aggregation induced by ristocetin (▶Fig. 1A, B), the inhibitory effect was readily enhanced by a low level of Gs stimulation with 6 nM PGE1 (▶Table 1). Notably enough, however, an absolute requirement of PGE1 was observed with K-134 at the therapeutic concentrations needed to inhibit VWF-dependent platelet thrombus formation under flow conditions (▶Figs. 2, 4). This discrepancy may be due to difference in threshold level of cAMP required to block intracellular signalling: one is ADP- and TXA_2-dependent GPIIb/IIIa activation pathway downstream of VWF-GPIb/V/IX interaction induced by ristocetin (aggregometer studies) and the other is secretion-independent integrin activation pathway induced by shear (flow chamber studies) ([23, 26] and ▶Figs. 1, 2, 6). Thus, our *in vitro* findings obtained under physiological flow conditions raised the notion that VWF-induced platelet thrombus formation may be efficiently blocked by PDE3 inhibitor under *in vivo* conditions where the endogenous Gs stimulators (PGI2 and adenosine) are up-regulated. As a matter of fact, considerable amounts of PGI2 were reportedly produced locally in response to mural platelet thrombus formation on de-endothelialised arterial wall (19). In addition, adenosine was released in hypoxic tissues during ischaemia and exerted ischaemic preconditioning effects (27, 28). Since both of these substances have very short biological lives *in vitro*, the stable PGI2 analogue, PGE1 may instead mimic the *in vivo* supporting effects on PDE3 inhibitor-driven suppression of VWF-dependent platelet thrombus formation under arterial shear conditions. Meanwhile, we speculated that there is no feasibility of clinical use of combined PDE3 inhibitor and Gs stimulator, since long-term administration of Gs stimulator leads to decreased sensitivity of human platelets to the drug (29).

What is known about this topic?

- Phosphodiesterase (PDE)3 inhibitor, cilostazol inhibits agonist-induced human platelet aggregation *ex vivo* but does not prolong bleeding time, and the risk of haemorrhage associated with treatment is quite low.
- Cilostazol neither increases cAMP levels of human platelets nor inhibits shear stress-induced platelet aggregation at therapeutic concentration in the absence of Gs stimulator *in vitro*.
- Cilostazol is not appropriate for *in vitro* experiments, because it is converted into several active metabolites *in vivo*.

What does this paper add?

- We investigated the anti-platelet mechanism of a more potent and selective PDE3 inhibitor, K-134, which is a cilostazol analog but not a pro-drug.
- Therapeutic concentrations of K-134 plus a low concentration of Gs stimulator synergistically increased platelet cAMP levels and strongly suppressed high shear-dependent platelet thrombus formation initiated by interactions between GPIb/V/IX and VWF but had much lower inhibitory effects under low shear than GPIIb/IIIa inhibitor or cyclooxygenase inhibitor.

Unlike tirofiban and ASA, PDE3 inhibitor does not prolong human bleeding time, even under repeated dosing, but exhibits significant inhibitory effects on agonist-induced platelet aggregation *ex vivo* (3, 4). Considering the observed high shear stress- and Gs stimulation-dependent antiplatelet effects of PDE3 inhibitor *in vitro* (▶ Figs. 4, 5), it may exert *in vivo* antiplatelet activity in a shear-dependent manner when concomitant stimulation of Gs-coupled receptors is induced at the site of arterial thrombosis and ischaemia. In contrast, tirofiban and ASA inhibit platelet aggregation regardless of shear and Gs stimulation, and thus may affect physiological haemostatic plug formation. To further understand the mechanism of their low risk of bleeding, we need to explore how the local concentrations of endogenous Gs stimulators are regulated at sites of vascular perturbation.

Care should be taken when the results of our *in vitro* perfusion experiments at a high shear rate of 1,500 s^{-1} are interpreted into the pathological conditions *in vivo*, since the regions of arterial stenosis are exposed to much higher shear rates ranging from 1,000 up to 10,000 s^{-1} (11). Nonetheless, considering the rebound phenomenon of Gs-stimulator (29), PDE3 may be a better drug-target to elevate platelet cAMP levels for the treatment of PAD (2) or secondary prevention of cerebral infarction (6) that needs long-term drug administration.

Acknowledgements

We thank Dr. A. Oda at Hokkaido University for valuable discussion and critical reading. This work was supported in part by Health and Labor Sciences Research Grants (Research on Public Essential Drugs and Medical Devices, M.H.) from the Ministry of Health, Labour and Welfare, Japan.

Conflict of Interest

The study was supported in part by a research grant from Kowa Company, Ltd. (Tokyo, Japan). H.Y. was an employee of Kowa Company, Ltd., Japan.

References

1. Feijge MA, Ansink K, Vanschoonbeek K, et al. Control of platelet activation by cyclic AMP turnover and cyclic nucleotide phosphodiesterase type-3. Biochem Pharmacol 2004; 67: 1559–1567.
2. Norgren L, Hiatt WR, Dormandy JA, et al.; TASC II Working Group. Inter-Society consensus for the management of peripheral arterial disease (TASC II). J Vasc Surg 2007; 45 (Suppl S): S5–67.
3. Kim JS, Lee KS, Kim YI, et al. A randomized crossover comparative study of aspirin, cilostazol and clopidogrel in normal controls: analysis with quantitative bleeding time and platelet aggregation test. J Clin Neurosci 2004; 11: 600–602.
4. Wilhite DB, Comerota AJ, Schmieder FA, et al. Managing PAD with multiple platelet inhibitors: the effect of combination therapy on bleeding time. J Vasc Surg 2003; 38: 710–713.
5. Hiatt WR, Money SR, Brass EP. Long-term safety of cilostazol in patients with peripheral artery disease: the CASTLE study (Cilostazol: A Study in Long-term Effects). J Vasc Surg 2008; 47: 330–336.
6. Gotoh F, Tohgi H, Hirai S, et al. Cilostazol stroke prevention study: a placebo-controlled double-blind trial for secondary prevention of cerebral infarction. J Stroke Cerebrovasc Dis 2000; 9: 147–157.
7. Savage B, Saldívar E, Ruggeri ZM. Initiation of platelet adhesion by arrest onto fibrinogen or translocation on von Willebrand factor. Cell 1996; 84: 289–297.
8. Savage B, Almus-Jacobs F, Ruggeri ZM. Specific synergy of multiple substrate-receptor interactions in platelet thrombus formation under flow. Cell 1998; 94: 657–666.
9. Kasirer-Friede A, Cozzi MR, Mazzucato M, et al. Signaling through GPIb/IX/V activates alpha IIb beta 3 independently of other receptors. Blood 2004; 103: 3403–3411.
10. Nieswandt B, Brakebusch C, Bergmeier W, et al. Glycoprotein VI but not alpha2beta1 integrin is essential for platelet interaction with collagen. EMBO J 2001; 20: 2120–2130.
11. Jackson SP, Nesbitt WS, Westein E. Dynamics of platelet thrombus formation. J Thromb Haemost 2009; 7 (Suppl 1):17–20.
12. Akiyama H, Kudo S, Shimizu T. The metabolism of a new antithrombotic and vasodilating agent, cilostazol, in rat, dog and man. Arzneimittelforschung 1985; 35: 1133–1140.
13. Minami N, Suzuki Y, Yamamoto M, et al. Inhibition of shear stress-induced platelet aggregation by cilostazol, a specific inhibitor of cGMP-inhibited phosphodiesterase, in vitro and ex vivo. Life Sci 1997; 61: PL 383–389.
14. Sudo T, Tachibana K, Toga K, et al. Potent effects of novel antiplatelet aggregatory cilostamide analogues on recombinant cyclic nucleotide phosphodiesterase isozyme activity. Biochem Pharmacol 2000; 59: 347–356.
15. Koga Y, Kihara Y, Okada M, et al. 2(1H)-quinolinone derivatives as novel anti-arteriostenotic agents showing anti-thrombotic and anti-hyperplastic activities. Bioorg Med Chem Lett. 1998; 8: 1471–1476.
16. Nishiya T, Kainoh M, Murata M, et al. Reconstitution of adhesive properties of human platelets in liposomes carrying both recombinant glycoproteins Ia/IIa and Ibα under flow conditions: specific synergy of receptor-ligand interactions. Blood 2002; 100: 136–142.
17. Shenkman B, Savion N, Dardik R, et al. Testing of platelet deposition on polystyrene surface under flow conditions by the cone and plate(let) analyzer: role of platelet activation, fibrinogen and von Willebrand factor. Thromb Res 2000; 99: 353–361.
18. Mazzucato M, Cozzi MR, Pradella P, et al. Distinct roles of ADP receptors in von Willebrand factor-mediated platelet signaling and activation under high flow. Blood 2004; 104: 3221–3227.
19. Tschopp TB, Baumgartner HR. Platelet adhesion and mural platelet thrombus formation on aortic subendothelium of rats, rabbits, and guinea pigs correlate negatively with the vascular PGI2 production. J Lab Clin Med 1981; 98: 402–411.
20. Sun B, Le SN, Lin S, et al. New mechanism of action for cilostazol: interplay between adenosine and cilostazol in inhibiting platelet activation. J Cardiovasc Pharmacol 2002; 40: 577–585.
21. Bodnar RJ, Xi X, Li Z, et al. Regulation of glycoprotein Ib-IX-von Willebrand factor interaction by cAMP-dependent protein kinase-mediated phosphorylation at Ser 166 of glycoprotein Ib(beta). J Biol Chem 2002; 277: 47080–47087.
22. Mazzucato M, Pradella P, Cozzi MR, et al. Sequential cytoplasmic calcium signals in a 2-stage platelet activation process induced by the glycoprotein Ibalpha mechanoreceptor. Blood 2002; 100: 2793–2800.
23. Yap CL, Hughan SC, Cranmer SL, et al. Synergistic adhesive interactions and signaling mechanisms operating between platelet glycoprotein Ib/IX and integrin alpha IIbbeta 3. J Biol Chem 2000; 275: 41377–41388.
24. Ichinohe T, Takayama H, Ezumi Y, et al. Cyclic AMP-insensitive activation of c-Src and Syk protein-tyrosine kinases through platelet membrane glycoprotein VI. J Biol Chem 1995; 270: 28029–28036.
25. Ryningen A, Jensen BO, Holmsen H. Role of autocrine stimulation on the effects of cyclic AMP on protein and lipid phosphorylation in collagen-activated and thrombin-activated platelets. Eur J Biochem 1999; 260: 87–96.
26. Liu J, Pestina TI, Berndt MC, et al. The roles of ADP and TXA_2 in botrocetin/VWF-induced aggregation of washed platelets. J Thromb Haemost 2004; 2: 2213–2222.
27. Pasini FL, Capecchi PL, Perri TD. Adenosine and chronic ischemia of the lower limbs. Vasc Med 2000; 5: 243–250.
28. Mubagwa K, Flameng W. Adenosine, adenosine receptors and myocardial protection: an updated overview. Cardiovasc Res 2001; 52: 25–39.
29. Sinzinger H, Silberbauer K, Horsch AK, et al. Decreased sensitivity of human platelets to PGI2 during long-term intraarterial prostacyclin infusion in patients with peripheral vascular disease--a rebound phenomenon? Prostaglandins 1981; 21: 49–51.

International Journal of Pharmaceutics 407 (2011) 151–157

Contents lists available at ScienceDirect

International Journal of Pharmaceutics

journal homepage: www.elsevier.com/locate/ijpharm

Pharmaceutical Nanotechnology

Decoration of fibrinogen γ-chain peptide on adenosine diphosphate-encapsulated liposomes enhances binding of the liposomes to activated platelets

Koji Tokutomi[a], Toshiaki Tagawa[b], Maki Korenaga[a], Masatoshi Chiba[a], Tomohiro Asai[c], Naohide Watanabe[d], Shinji Takeoka[e], Makoto Handa[d], Yasuo Ikeda[e], Naoto Oku[c,*]

[a] Pharmaceutical Research Department of CMC Research Center, Mitsubishi Tanabe Pharma Corporation, 3-16-89, Kashima, Yodogawa-ku, Osaka 532-8505, Japan
[b] Medicinal Chemistry Research Laboratories 1 Research Division, Mitsubishi Tanabe Pharma Corporation, 1000, Kamoshida, Aoba-ku, Yokohama, Kanagawa 227-0033, Japan
[c] Department of Medical Biochemistry and Global COE Program, Graduate School of Pharmaceutical Sciences, University of Shizuoka, 52-1 Yada, Suruga-ku, Shizuoka 422-8526, Japan
[d] Department of Transfusion Medicine and Cell Therapy, Keio University School of Medicine, 35 Shinanomachi, Shinjuku-ku, Tokyo 160-8582, Japan
[e] Department of Life Science and Medical Bioscience, Graduate School of Advanced Science and Engineering, Waseda University, TWIns, 2-2 Wakamatsu, Shinjuku-ku, Tokyo 162-8480, Japan

ARTICLE INFO

Article history:
Received 2 November 2010
Received in revised form
14 December 2010
Accepted 4 January 2011
Available online 18 January 2011

Keywords:
Hemostasis
Liposome
Fibrinogen
Platelet aggregation
ADP

ABSTRACT

For the purpose of efficient hemostasis, we previously developed ADP-encapsulated liposomes modified with a dodecapeptide (HHLGGAKQAGDV, H12), H12-(ADP)Lipo. This liposome actually enhanced platelet aggregation *in vitro*, and showed significant hemostatic effect *in vivo*. Since fibrinogen (Fbg) is abundant in the bloodstream, it is unclear why this liposome binds platelets so efficiently, overcoming the competition with Fbg. Therefore, we investigated the relationship between H12 density on the liposome and the binding ability to platelets, and evaluated the inhibitory effect of Fbg on the binding of H12-(ADP)Lipo to platelets. As a result, the binding ability to platelets steeply increased depending on H12 density until it reached about 3×10^{15} H12 molecules/m^2. The 50% inhibition concentration of Fbg on the binding of H12-(ADP)Lipo to platelets was about 25-fold over the concentration of H12 molecules on the liposome. Moreover, almost no inhibition by Fbg was observed at the physiological concentration of it. This result suggests that the ability of H12 to bind to GPIIb/IIIa increased overwhelmingly by the anchoring to the liposome that enabled the cooperative binding of H12 peptides to the platelets.

1. Introduction

Recently, strong chemotherapy and bone-marrow transplantation techniques have appeared as a treatment method for malignant tumors and disorders of the hematopoietic system. Since these treatments often are accompanied by a decrease in the platelet count, the importance of platelet transfusion has come to be recognized as a supportive therapy. However, there are two serious problems with platelet transfusion. One of them is the short supply caused by the short storage life of platelets (4 days in Japan, 5–7 days in USA and Europe). The other is the side effects such as transfusion-transmitted diseases and immune reactions. To solve these problems, various platelet substitutes (Blajchman, 2003), which consist of materials derived from blood components, have been developed, such as solubilized platelet membrane protein-conjugated liposomes, plateletsome (Rybak and Renzulli, 1993); infusible platelet membranes, IPM (Graham et al., 2001); fibrinogen-coated albumin microcapsules, synthocyte (Levi et al., 1999); fibrinogen-bonded red blood cells (Agam and Livine, 1992); liposome-bearing fibrinogen (Casals et al., 2003); arginine–glycine–aspartic acid (RGD) peptide-bound red blood cells, thromboerythrocyte (Coller et al., 1992). Some of these make platelet-like aggregates, and others enhance platelet aggregation.

In the circulation, platelet aggregation is mediated by fibrinogen, which bridges adjacent platelets through integrin αIIbβIII (GPIIb/IIIa) on the platelet surface in an activation-dependent manner. We have developed platelet substitutes using liposome modified with dodecapeptide (HHLGGAKQAGDV, H12) as biodegradable carriers for the purpose of enhancing platelet aggregation. H12 peptide is a fibrinogen γ-chain carboxyl-terminal sequence (γ400–411) and recognizes specifically the active form of GPIIb/IIIa on the surface of activated platelets. Other sequences in fibrinogen have been designated as GPIIb/IIIa recognition sites: the RGD-based sequences ^{95}RGDF^{98} and ^{572}RGDS^{575} in the Aα-chain (Andrieux et al., 1989). Whereas, RGD-related peptides interact with many integrins expressed in various types of cells, H12 peptide

* Corresponding author. Tel.: +81 54 264 5701; fax: +81 54 264 5705.
E-mail address: oku@u-shizuoka-ken.ac.jp (N. Oku).

0378-5173/$ – see front matter © 2011 Elsevier B.V. All rights reserved.
doi:10.1016/j.ijpharm.2011.01.014

has high specificity toward GPIIb/IIIa on platelets (Ruoslahti et al., 1996). In fact, H12-coated polymerized albumin and H12-coated polyethylene glycol-modified liposomes show specific interaction with activated platelets, augment platelet-mediated thrombus formation on collagen-immobilized surfaces under flow condition *in vitro*, and prolong hemostatic ability *in vivo* to correct bleeding time in a dose-dependent manner in thrombocytopenic rat and rabbit models (Okamura et al., 2005a,b, 2007).

To strengthen the hemostatic ability of the H12-coated liposome (H12-Lipo) as a platelet substitute, we exploited its drug delivery function by encapsulating adenosine diphosphate (ADP), potent platelet agonist, into the liposomes, referred to as H12-(ADP)Lipo. In fact, H12-(ADP)Lipo was more effective than H12-Lipo or liposome encapsulating ADP without surface modification (ADP)Lipo, for platelet aggregation *in vitro* and for hemostasis *in vivo* (Okamura et al., 2009). It is known that a large amount of fibrinogen (Fbg), approximately 200 mg/dL, is present in normal human blood (Halle et al., 1996), which would be expected to compete with H12 peptide for the binding to GPIIb/IIIa (Kloczewiak et al., 1984), as the affinity of Fbg for GPIIb/IIIa on platelets is known to be higher than that of H12 peptide (Timmons et al., 1984; Ruggeri et al., 1986). Therefore, the enhancing effect of H12-(ADP)Lipo on platelet aggregation and hemostasis means that H12-(ADP)Lipo overcomes the inhibition by Fbg and effectively binds to GPIIb/IIIa on platelets.

However, it is not yet clear how H12-(ADP)Lipo overcomes the inhibition by a large amount of Fbg. We thought that H12 density on liposomal surface greatly contributed to the binding ability to platelets. Therefore, in this study, we explored the relationship between the amount of H12 modification of liposomes and the platelet-binding ability of these liposomes, and evaluated the ability of H12-(ADP)Lipo to bind to platelets in the presence of Fbg at physiological concentration or more.

2. Materials and methods

2.1. Materials

1,2-Dipalmitoyl-sn-glycero-3-phosphocholine (DPPC), cholesterol, and 1,5-dihexadecyl-N-succinyl-L-glutamate (DHSG, Chart 1) were purchased from Nippon Fine Chemical Co. Ltd. (Osaka, Japan) and 1,2-distearoyl-sn-glycero-3-phosphatidylethanolamine-N-[monomethoxypoly(ethyl-eneglycol)] (PEG-DSPE, 5.1 kDa) and MalPEG3400-DSPE were from NOF Co. Ltd. (Tokyo, Japan). Cys-coupled fibrinogen γ-chain dodecapeptide (C-HHLGGAKQAGDV, Cys-H12) was synthesized by GL Biochem. (Shanghai, China) on consignment contract. H12-MalPEG3400-DSPE was synthesized in our laboratory (Chart 1). Adenosine 5′-diphosphate sodium salt (ADP), prostaglandin E1 (PGE_1), fibrinogen from human plasma, poly-L-lysine hydrobromide, decaethylene glycol monododecyl ether ($C_{12}E_{10}$), and HEPES were purchased from Sigma (St. Louis, MO, USA). Thrombin receptor activator for peptide-6 amide trifluoroacetate salt (SFLLRN-amide, TRAP) was obtained from Bachem AG (Bubendorf, Switzerland). Anti-human fibrinogen, FITC-conjugated was obtained from Millipore (Victoria, Australia). 3,3′-Dioctadecyloxacarbocyanine perchlorate ($DiOC_{18}$) was purchased from Invitrogen Co. (Eugene, OR, USA). Sephadex G25 for gel permeation chromatography (GPC) came from GE Healthcare (Buckinghamshire, UK).

2.2. Preparation of non-modified and H12-modified liposomes (H12-Lipo)

DPPC (665 mg, 0.91 mmol), cholesterol (350 mg, 0.91 mmol), DHSG (126 mg, 181 μmol), and PEG-DSPE (31 mg, 5.5 μmol) were dissolved in benzene 25 mL, and it divided equally to five. H12-PEG-DSPE (50 mg, 9.2 μmol) dissolved in methanol 20 mL. 0, 0.6, 1.1, 2.2, 4.4 or 8.8 mL of H12-PEG-DSPE in methanol solution was mixed with the former five benzene solution to prepare DPPC/cholesterol/DHSG/PEG-DSPE/H12-PEG-DSPE liposomes (5/5/1/0.03/0, 0.02, 0.03, 0.06, 0.12, and 0.24 as molar ratio), which were then freeze-dried. The mixed lipids were hydrated with phosphate-buffered saline (PBS, pH 7.4) for 3 h at 25 °C, and extruded through membrane filters with 0.45 μm and 0.22 μm pores (Durapore; Millipore Co., Tokyo, Japan). The liposomes thus obtained were washed with PBS by centrifugation (100,000 × *g* for 30 min at 4 °C). $DiOC_{18}$ in DMSO (2 mM), a hydrophobic fluorescent compound, was added to the each liposome suspension, and incubated for 5 min at 25 °C. Unincorporated $DiOC_{18}$ and DMSO were removed by use of GPC.

2.3. Preparation of H12-modified ADP-encapsulated liposomes, H12-(ADP)Lipo

DPPC (665 mg, 0.91 mmol), cholesterol (350 mg, 0.91 mmol), DHSG (126 mg, 181 μmol), PEG-DSPE (31 mg, 5.5 μmol), and H12-PEG-DSPE (30 mg, 5.5 μmol) (5/5/1/0.03/0.03 as the molar ratio) were dissolved in 6.5 mL ethanol/methanol (6/7, v/v) and a partial of the solution was injected into an aqueous solution 40 mL to form liposomes. Then, the liposomal solution was sonicated at 60 °C, freeze–thawed by using liquid N_2, and freeze-dried. The dried liposomes were rehydrated with PBS containing 2 mM ADP with sonication at 60 °C and extruded through membrane filters having pore sizes of 0.45 and 0.22 μm. The remaining ADP was removed, and the liposomal suspension was concentrated by tangential flow filtration. A DMSO solution of $DiOC_{18}$ (2 mM) was added to the liposome suspension, and the suspensions were incubated at 25 °C for 5 min. The $DiOC_{18}$-labeled liposomes were collected by GPC.

2.4. Characterization of the liposomes

The particle size was measured by using a dynamic light-scattering method (FPAR-1000; Otsuka Electric Co. Ltd., Osaka, Japan). The zeta-potential of the liposomes was determined with an electrophoretic light-scattering apparatus (ELS-8000; Otsuka Electric Co. Ltd.). The amount of ADP in the liposomal suspension was measured as follows: liposomes were added to PBS containing 8% $C_{12}E_{10}$ and incubated at 50 °C for 5 min, and then sonicated for 10 min. ADP was measured by HPLC (Shimadzu Co., Kyoto, Japan)

a DHSG

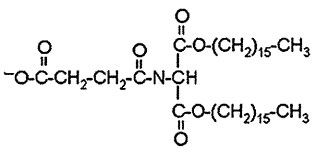

b H12-MALPEG3400-DSPE

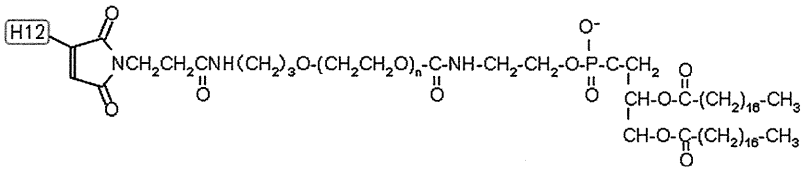

Chart 1. Structure of liposome contents. (a) 1,5-Dihexadecyl-N-succinyl-L-glutamate. (b) H12 is the fibrinogen γ chain (γ400–411) His-His-Leu-Gly-Gly-Ala-Lys-Gln-Ala-Gly-Asp-Val.

and an ultra violet detector. The density of each component of liposomal lipids was measured by HPLC and a corona charged aerosol detector (CAD; ESA Bioscience Inc., Chelmsford, USA). $DiOC_{18}$ introduced into liposome was measured as follows: $DiOC_{18}$-labeled liposomes were added to isopropanol and incubated at 45 °C for 10 min. The fluorescence intensity of $DiOC_{18}$ eluted from the liposomes was measured by using a micro-plate reader (Multimode plate reader SPECTRAmaxM2; Molecular Devices, CA, USA).

Lamellarity, the average number of bilayer membranes of the liposomes, was calculated from the volume ratio of liposomes in the suspension. Liposomes were mixed with a poly(ethylene oxide) solution (MW = 100 kDa, final concentration, 12 mg/mL) and a poly-L-lysine hydrobromide solution (final concentration, 1.8 mg/mL). The volumes of the liposomal suspension, a poly(ethylene oxide) solution, and a poly-L-lysine hydrobromide solution were 120 μL, 40 μL and 3 μL, respectively. The liposomes were precipitated by hematocrit centrifugation (15,000 × *g* for 30 min at 25 °C) to measure their volume ratio. Lamellarity (*N*) was calculated by using Eq. (1); H12 density on the liposomal surface (D_{H12}), by using Eq. (2).

$$N = \frac{AV(C \times 10^{-3})R_{dil}N_A}{2SR \times 10^{-8}} \quad (1)$$

$$D_{H12} = \frac{V(C_{H12} \times 10^{-3})R_{dil}N_A}{2SRN \times 10^{-8}} \quad (2)$$

where the volume and surface area of single liposomes calculated from the average diameter are V (m^3) and S (m^2), the volume ratio of liposomes in the suspension and lipid concentration are R (%) and C (M), and the surface area of a lipid molecule is A (m^2). N_A is the Avogadro constant (6.0×10^{23}). R_{dil} is the dilution ratio of the liposomal suspension (120/163).

2.5. Flow cytometry for detection of Fbg binding to TRAP-activated platelets

Blood withdrawn from healthy volunteers was mixed with a 10% volume of 3.8% sodium citrate. Platelet-rich plasma (PRP) was prepared by centrifugation of the blood (100 × *g* for 15 min at 25 °C). PRP was mixed with a 15% volume of acid–citrate–dextrose solution composed of 2.2% sodium citrate, 0.8% citric acid, and 2.2% glucose (ACD) containing 1 μM PGE_1. The suspension was centrifuged (2200 × *g* for 7 min at 25 °C), and the plasma was replaced with Ringer's-citrate–dextrose solution (RCD solution, composition: 0.76% citric acid, 0.090% glucose, 0.043% $MgCl_2$, 0.038% KCl, 0.60% NaCl; pH 6.5) containing 1 μM PGE_1. After the pellets had been resuspended in RCD solution, the suspension was centrifuged (2200 × *g* for 7 min at 25 °C); the concentrated platelets were then resuspended at 1.0×10^5 cells/μL in a modified HEPES–Tyrode buffer (137 mM NaCl, 0.42 mM NaH_2PO_4, 2.7 mM KCl, 12 mM $NaHCO_3$, 2 mM $MgCl_2$, 10 mM HEPES [N-2-hydroxyethylpiperazine-N-2-ethanesulfonic acid], and 0.1% glucose; pH 7.4). The platelet count was determined by using an automated hematology analyzer (K-4500, Sysmex Co., Kobe, Japan).

Anti-human fibrinogen, FITC-conjugated (FITC-Fbg) was added to the washed platelets (1.0×10^5 cells/μL). TRAP with various concentrations (final concentrations, 0–100 μM) were added to the suspension to activate the platelets, and the suspension was then incubated at 37 °C for 10 min before fixation with formaldehyde (final concentration, 1.8%, v/v). The mixture was incubated in darkness (15 min at 25 °C), and added to H–T buffer (1 mL). The platelets were gated to their characteristic forward versus side scatter, and 10,000 platelets were analyzed by using a FACSCalibur flow cytometer (Nippon Becton Dickinson Co., Tokyo, Japan). The platelet binding with the fibrinogen was quantified as the fraction of the fluorescent-positive platelets.

2.6. Flow cytometry of H12-Lipo binding to activated platelets

The washed platelets were prepared as described in Section 2.5 above. $DiOC_{18}$-labeled H12-Lipo (final concentration, 0.5 mg/mL) was added to the washed platelets (1.0×10^5 cells/μL). TRAP of various concentrations (final concentration, 0–50 μM) was added to the suspension to activate the platelets, and the suspension was then incubated at 37 °C for 10 min before fixation with formaldehyde. The mixture was incubated in darkness (15 min at 25 °C), and then added to H–T buffer (1 mL). The platelets were gated to their characteristic forward versus side scatter, and 10,000 platelets were analyzed by using the FACSCalibur flow cytometer. The platelet binding with the liposomes was quantified as the fraction of the fluorescent-positive platelets.

The mean fluorescence intensity (MFI) was calculated by using Eq. (3), and was the indicator of the relative amount of liposomes bound to a platelet cell. MFI was used as an index of the binding ability.

$$\text{MFI} = \frac{\sum(\text{FL1-H} \times \text{count})}{\text{total count}} \quad (3)$$

FL1-H, fluorescence intensity; count, number of cells with each fluorescence intensity; total count, detected number of all cells.

Average (n=3) MFI of the non-stimulated group was subtracted from each MFI as background. Each $DiOC_{18}$ fluorescence was divided by the lipid amount (w/w, %).

2.7. Inhibitory effect of Fbg on H12-(ADP)Lipo binding to activated platelets

The washed platelets were prepared as described in Section 2.5. $DiOC_{18}$-labeled H12-(ADP)Lipo (final concentration, 0.5 mg/mL) and Fbg from human plasma (final concentration, 6 μM) were added to the washed platelets (1.0×10^5 cells/μL). TRAP (0–50 μM) was added to the suspension to activate the platelets, and the suspension was then incubated at 37 °C for 10 min. H12-(ADP)Lipo bound to the activated platelets was determined as described in Section 2.6.

In another experiment, $DiOC_{18}$-labeled H12-(ADP)Lipo and various concentrations of Fbg (0–60 μM) were added to the washed platelets, which were then activated with 30 μM TRAP for 10 min at 37 °C. The 50% inhibition concentration of Fbg for blocking the binding of H12-(ADP)Lipo (0.5 mg/mL as lipids) to the platelets was determined by using the analytical software Graph Pad Prism 5J. The MFI of the TRAP-added group was assumed to be 100% binding, and that without the TRAP-treated group was assumed to be 0% binding.

In this study, the final liposomal concentration was fixed at 0.5 mg/mL as lipids during incubation with platelets. Therefore, the calculated H12 concentration in the incubation mixture of H12-(ADP)Lipo was 2.3 μM. This value well correlated with the concentration of H12 peptide obtained from lipid analysis, which was about 2 μM (data not shown).

2.8. Statistical analysis

Statistical analysis was carried out by Student's *t*-test.

3. Results

3.1. Physicochemical characteristics of the liposomes

We prepared vacant liposomes without (plain-liposomes) or with various amounts of H12-PEG-DSPE (H12-Lipo), as well as H12-modified ADP-encapsulated liposomes, H12-(ADP)Lipo. The physicochemical characteristics of the various liposomes are

Table 1
Physicochemical characteristics of the liposomes.

	Plain-Lipo	H12-Lipo (0.006)	H12-Lipo (0.014)	H12-Lipo (0.036)	H12-Lipo (0.065)	H12-Lipo (0.175)	H12-(ADP)Lipo
Particle size (nm)	314.8	303.8	301.2	299.3	294.2	245.6	295.4
Polydispersity index	0.132	0.130	0.183	0.180	0.126	0.107	0.187
ζ-Potential (mV)	−12.26	−7.77	−5.46	−3.66	−4.72	−4.13	−7.70
ADP (μg/mL)	–	–	–	–	–	–	14.17
Molar ratio							
DPPC	4.975	4.972	4.845	4.959	5.137	5.341	4.836
Cholesterol	5.000	5.000	5.000	5.000	5.000	5.000	5.000
DHSG	0.929	0.910	0.906	0.910	0.940	0.987	0.937
PEG5000-DSPE	0.025	0.025	0.025	0.025	0.025	0.025	0.025
H12-PEG-DSPE	–	0.006	0.014	0.036	0.065	0.174	0.023
Lamellarity	1.20 ± 0.05	0.94 ± 0.02	0.95 ± 0.01	1.06 ± 0.01	1.01 ± 0.01	1.02 ± 0.02	0.97 ± 0.01
H12 density × 10^{15} (molecules/m^2)	0	1.32	2.93	8.15	13.8	35.9	4.91

DPPC/cholesterol/DHSG/PEG-DSPE with H12-PEG-DSPE liposomes (5/5/1/0.03 with 0 (plain-Lipo), 0.02, 0.03, 0.06, 0.12, and 0.24 as the molar ratio) was prepared, and the actual amount of each component after preparation was determined. The relative amount was expressed where the cholesterol content was assumed to be 5.000. Lamellarity is shown as the mean ± SD (n = 3).

shown in Table 1. The particle sizes were about 300 nm in diameter except for H12-Lipo (0.175), the diameter of which was about 250 nm. Lamellarity of all liposomes tested was calculated by using Eq. (1) shown in Section 2.4 and was about 1.0, indicating that these liposomes were unilamellar vesicles. The H12 density on the liposomal surface was calculated by using Eq. (2) described in Section 2.4 and N = 1 was applied.

The morphology of H12-(ADP)Lipo was observed by electron microscopy (Fig. 1): the liposomal size observed by TEM was almost the same as that measured by the dynamic light-scattering method, although the size was not homogeneous. Moreover, H12-(ADP)Lipo was mostly unilamellar or oligolamellar vesicles.

3.2. *Effect of H12-modification of the liposomes on their binding to platelets*

To evaluate the ability of H12-modified liposomes to bind to activated platelets, we firstly examined Fbg binding to platelets that had been activated with TRAP, a protease-activated receptor (PAR) 1 agonist and an activator of platelets and GPIIb/IIIa. The amount of FITC-Fbg bound to human platelets well correlated with the TRAP stimulation, and the increase in binding nearly reached its plateau at 30 μM TRAP (Fig. 2). It is known that Fbg binds to the activated GPIIb/IIIa on the platelet surface through the H12 peptide sequence, HHLGGAKQAGDV, located at the carboxyl-terminus of the fibrinogen γA chain (γ400–411), and through the RGD motifs presenting in a fibrinogen Aα chain (Aα95–97, Aα572–574). Fbg is present in the blood as a dimeric form, and the dimer has 2 H12 sites and 4 RGD sites as ligands for GPIIb/IIIa (Michael, 1990, 1992) suggesting that Fbg binds to platelets in a multivalent fashion.

Next, by FACS analysis we measured the ability of the $DiOC_{18}$-labeled liposomes bearing various amounts of H12 to bind to TRAP-activated platelets. The mean fluorescence intensity (MFI)

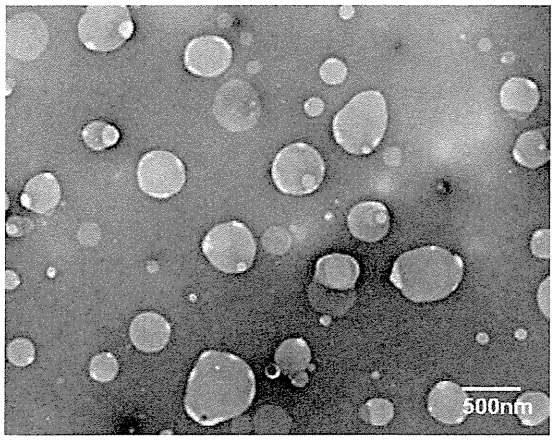

Fig. 1. TEM image of H12-(ADP)Lipo. This liposome sample was suspended on a transmission electron microscopic grid coated with collodion film, stained with phosphotungstic acid, and then examined with a Hitachi H-9000UHR type transmission electron microscope operated at 100 kV.

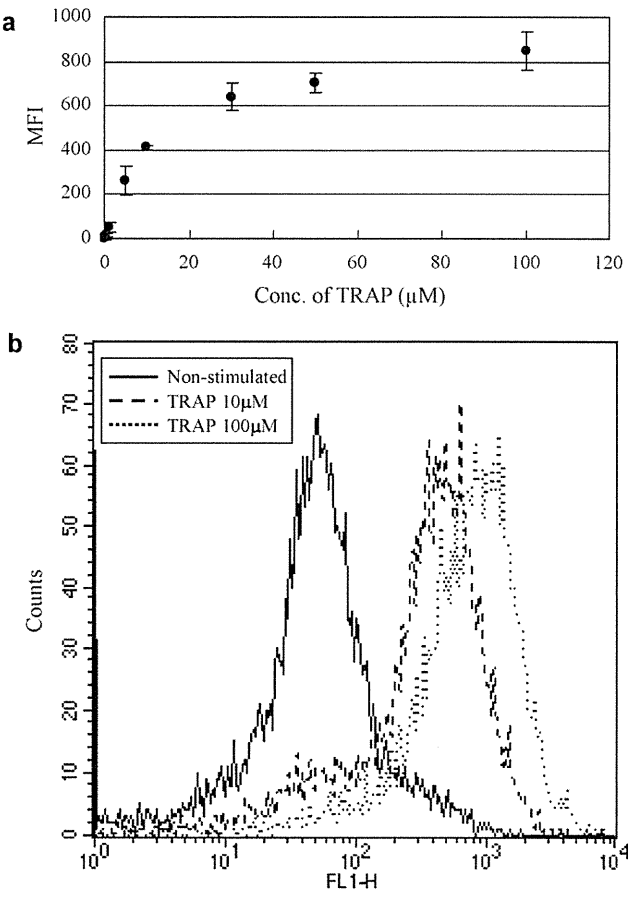

Fig. 2. TRAP-induced activation of GPIIb/IIIa on platelets. (a) Various concentrations of TRAP (0–100 μM) were added to washed platelets (platelet = 1.0 × 10^5 cells/μL, 80 μL) in the presence of FITC-Fbg, and incubated at 37 °C for 10 min before fixation with formaldehyde (1.8%, v/v). The mixture was incubated in the darkness (15 min at 25 °C), and mixed with H–T buffer (1 mL). The platelets were gated to their characteristic forward versus side scatter, and 10,000 platelets were analyzed by using a flow cytometer. FITC-Fbg binding to platelets was quantified as the fraction of fluorescent-positive platelets. Data are expressed as the mean ± SD (n = 3). (b) Each histogram represents the binding of FITC-Fbg to human platelets non-stimulated, stimulated by 10 μM TRAP or 100 μM TRAP.

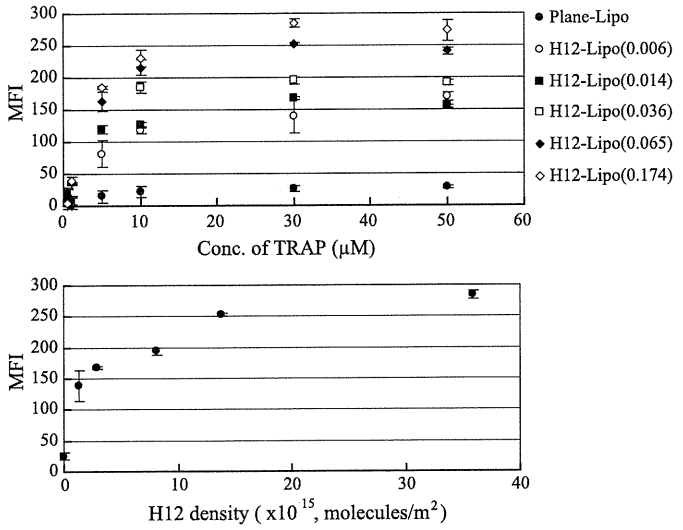

Fig. 3. Effect of modification of liposomes with H12 on their ability to bind to platelets. Liposomes modified with various amounts of H12 peptide were prepared. Each liposomal sample (0.5 mg/mL lipids) labeled with $DiOC_{18}$ was incubated with washed platelets (platelet = 1.0×10^5 cells/μL, 80 μL) at 37 °C for 10 min in the presence of various amounts of TRAP. Then the platelets were fixed with formaldehyde (1.8%, v/v), incubated in the darkness (15 min, 25 °C), and mixed with H–T buffer (1 mL). The platelet samples were then examined by flow cytometry. The liposomes bound to platelets were quantified as the fraction of fluorescent-positive platelets. Data are expressed as the mean ± SD ($n = 3$). (a) The relative binding of H12-Lipo to platelets activated with various concentrations of TRAP. The H12 molar ratios of each liposome to cholesterol (assumed to be 5) were 0 (●), 0.006 (○), 0.014 (■), 0.036 (□), 0.065 (♦) and 0.174 (◇), respectively. (b) The relative binding of liposomes with various H12 density to platelets activated with 30 μM TRAP.

was used as an index of the binding ability. As a result, the binding of the liposomes to the platelets increased in a TRAP concentration-dependent manner and reached its plateau at the TRAP concentration of 30 μM (Fig. 3a). Fig. 3b shows the relationship between MFI and H12 density on the liposomal surface when the platelets were activated with 30 μM TRAP. The binding ability of the liposomes increased depending on the H12 density of the liposomes and reached its plateau at the calculated H12 density of 1.38×10^{16} molecules/m^2.

3.3. *Inhibitory effect of fibrinogen on the binding of H12-(ADP)Lipo to platelets*

The concentration of Fbg in normal human blood is about 200 mg/mL (5.9 μM) and Fbg is known to bind to activated GPIIb/IIIa on platelets (Halle et al., 1996) and would be expected to act as an inhibitor of H12-(ADP)Lipo binding to platelets. Therefore, by FACS analysis we evaluated the ability of H12-(ADP)Lipo (H12 density: 4.9×10^{15} molecules/m^2) to bind to activated platelets in the presence or absence of Fbg. The physiological concentration of Fbg (6 μM) inhibited the liposomal binding only partially at all TRAP concentrations tested (Fig. 4): the maximum inhibition (about 18.8%) was observed at 30 μM TRAP stimulation, where the MFI in the presence or absence of Fbg were 404 ± 32 and 304 ± 6, respectively. Furthermore, the inhibition ratios at 5 or 1 μM TRAP were 8.8% or 1.4%, respectively, suggesting that the effect of Fbg on liposomal binding to platelets was hardly observed in a low activation state of platelets. It is thought that only a small amount of activated GPIIb/IIIa is present on the surface of platelets in the low activation state.

To evaluate the specificity of H12-(ADP)Lipo binding to GPIIb/IIIa, we investigated the competitive inhibition of the liposomal binding to activated platelets in the presence of excess Fbg.

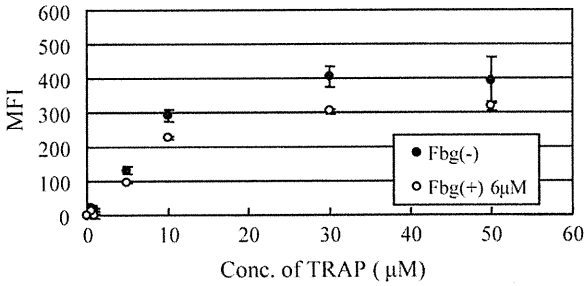

Fig. 4. H12-(ADP)Lipo binding to platelets in the presence of the physiological concentration of fibrinogen. H12-(ADP)Lipo labeled with $DiOC_{18}$ (0.5 mg/mL as lipids) and various concentrations of TRAP (0–50 μM) without (●) or with 6 μM Fbg (○) were added to washed platelets (1.0×10^5 cells/μL, 80 μL). The suspension was incubated at 37 °C for 10 min before fixation with formaldehyde (1.8%, v/v). Liposomal fluorescence associated with platelets was determined. Data are expressed as the mean ± SD ($n = 3$).

The binding of H12-(ADP)Lipo to platelets was inhibited in the presence of excess concentrations of Fbg, and about 90% inhibition was observed at 60 μM Fbg (Fig. 5a). This finding suggests that H12-(ADP)Lipo bound to a specific site on activated platelets, that is, the same site for Fbg binding, namely, GPIIb/IIIa. The 50% inhibition concentration of Fbg for blocking the binding of H12-(ADP)Lipo (final concentration, 0.5 mg/mL) was calculated by using analytical software Graph Pad Prism 5J: Fig. 5b shows the fitting-curve of the inhibition. As a result, the 50% inhibition concentration of Fbg was 25.2 μM, about 4.3-fold higher than its blood level.

4. Discussion

The purpose of our study was to focus on the utility of H12-modified ADP-encapsulated liposomes, H12-(ADP)Lipo, as a hemostat. We previously reported that H12-(ADP)Lipo enhances the platelet aggregation in PRP and significantly reduces the bleeding times in thrombocytopenic rat and rabbit models and that H12-(ADP)Lipo is more efficient than H12-Lipo or (ADP)Lipo (Okamura et al., 2005a,b, 2007). It is thought that the hemostatic effect of H12-(ADP)Lipo is based on the following sequential events: binding to activated platelets, releasing ADP that further activates platelets to form a thrombus, and bridging platelets to make large aggregates for hemostasis.

The H12 peptide is derived from a fibrinogen γ chain carboxyl-terminal sequence and has the binding ability to activated GPIIb/IIIa on platelets (Michael, 1990, 1992). Therefore, the hemostasis induced by H12-(ADP)Lipo mimics the hemostasis with Fbg and platelets. In fact, platelet aggregation is induced by a large amount of Fbg and von Willebrand Factor (vWF) in blood (Takagi et al., 2002). Since H12 and Fbg share the same target, namely, activated GPIIb/IIIa, it is necessary that H12-(ADP)Lipo overcomes the competition with Fbg and binds to platelets for inducing enhanced hemostasis. However, the effect of Fbg on the binding of H12-(ADP)Lipo to platelets had not been evaluated previously. In this study, by using FACS analysis, we evaluated the effect of the presence of Fbg on the binding of H12-(ADP)Lipo to platelets.

It is known that GPIIb/IIIa is a resting form on non-stimulated platelets and is converted to its active form upon stimulation of platelets. The active GPIIb/IIIa exposes the Fbg-binding sites to which the H12 peptide binds (Du et al., 1991). Firstly, we examined the change in the activation level of platelets depending on the stimulation with TRAP, a platelet-activating agent. As a result, it was clear that GPIIb/IIIa activation depended on the TRAP concentration (Fig. 2). Next, we examined the influence of the H12 density on the liposomal surface under various stimulation conditions by

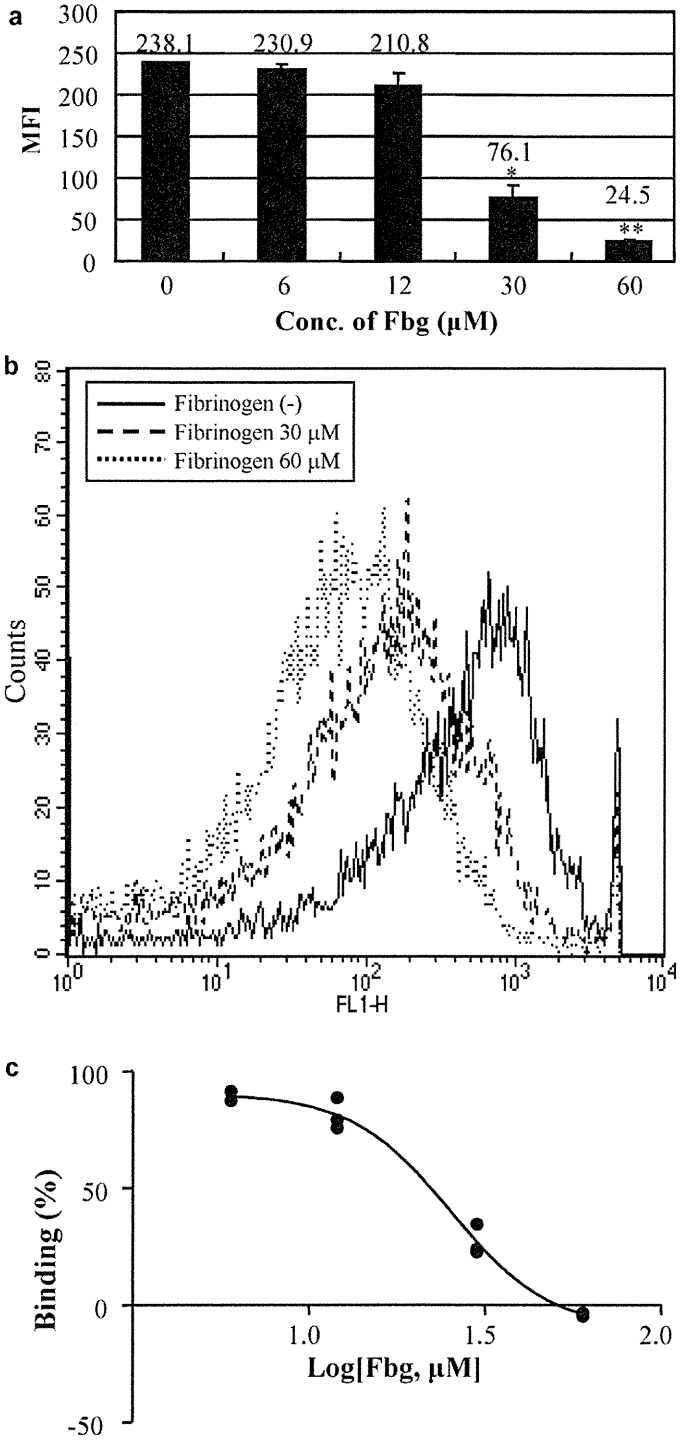

Fig. 5. Inhibitory effect of fibrinogen on the binding of H12-(ADP)Lipo to platelets. (a) H12-(ADP)Lipo labeled with $DiOC_{18}$ (0.5 mg/mL), 30 μM TRAP, and various concentrations of Fbg were added to washed platelets (1.0×10^5 cells/μL, 50 μL). Significant difference from Fbg 0 μM group are indicated by $^*P < 0.01$ and $^{**}P < 0.001$. The suspension was then incubated at 37 °C for 10 min before fixation with formaldehyde. Liposomes associated with platelets were analyzed fluorometrically by using flow cytometry. Data are expressed as the mean ± SD ($n = 3$). (b) Each histogram represents the binding of H12-(ADP)Lipo to human platelets stimulated by 30 μM TRAP with Fbg (30 μM) or Fbg (60 μM). (c) The curve for inhibition by Fbg of binding of H12-(ADP)Lipo to platelets was fitted by using the Graph Pad Prism 5J. The mean Fl of Fbg(−) TRAP-added group was assumed to be 100% binding; that without TRAP-treatment group, 0% binding.

varying the TRAP concentration. The ability of H12-Lipo to bind to the platelets increased depending on the H12 density of the liposomal surface and the TRAP concentration (Fig. 3a). At the low level of H12 density on the liposomes ($<2.9 \times 10^{15}$ molecules/m^2), the binding ability increased depending on the increase in H12 density, and it nearly reached the plateau at an H12 density of about 1.4×10^{16} molecules/m^2 (Fig. 3b).

On the other hand, GPIIb/IIIa, one of the most predominant glycoproteins on platelets, is present as approximately 5×10^4 molecules/platelet in healthy blood. Platelets are smaller than other cells, and the size of platelets is assumed to be 2 μm in diameter (Milton et al., 1985; Kuwahara et al., 2002). Therefore, if the platelet is assumed to be spherical, the density of GPIIb/IIIa on the platelet cell surface is 4.0×10^{15} molecules/m^2, although actual platelets were not spherical shape at the aggregated site.

Considering the data in Fig. 3, it seems that the binding ability of H12-Lipo is sensitively changed according to the H12 density when the H12 density on the liposome is lower than the GPIIb/IIIa density on the platelet surface (4.0×10^{15} molecules/m^2, when 30 μM TRAP is assumed to activate all GPIIb/IIIa molecules). On the contrary, when the H12 density on the liposomal surface becomes higher ($>1.4 \times 10^{16}$ molecules/m^2) than that of GPIIb/IIIa on the platelet, it seems that the change in the binding ability is not sensitive to the change in the H12 density. Taken together, the H12 density on the liposomal surface is an important factor for the binding of the liposomes to platelets, and the H12 peptide on the liposomal surface may act cooperatively in binding of the H12-Lipo to GPIIb/IIIa on the platelet.

The activation level of platelets at the site of a vascular injury may be dependent on the level of wounding. Therefore, we evaluated the binding ability of H12-(ADP)Lipo over a wide range of activation level of platelets (Fig. 4) in the presence of the physiological concentration of Fbg, namely, 6 μM. This concentration of Fbg did not suppress much the binding of the liposome to platelets because H12-(ADP)Lipo had a multivalent effect of H12 peptide enough for the inhibition effect of Fbg. Furthermore, this result suggested that H12-(ADP)Lipo may overcome the inhibition of Fbg over a wide range of platelet activation levels *in vivo*. The site of binding of H12-(ADP)Lipo to GPIIb/IIIa was confirmed to be the same as that of Fbg, since the binding was almost completely blocked by the high concentration of Fbg (Fig. 5a).

The 50% inhibition concentration of Fbg to block the binding of H12-(ADP)Lipo (final concentration, 0.5 mg/mL as lipids) to platelets was approximately 25 μM under the present experimental conditions (Fig. 5a). Since the concentration of H12 peptide in the reaction liquid was calculated to be about 2 μM, H12 peptide exposed on the surface of liposome was assumed to be about 1 μM in consideration of liposomal lamellarity (approximately 1.0): one-half of the H12 is assumed to be present in the outer leaflet of the lipid bilayer, and another one-half in the inner leaflet of the bilayer. Moreover, it was known that Fbg forms a dimer and that 1 molecule of Fbg has 2 H12 peptide sequences and 4 sites of RGD sequence (Michael, 1990, 1992). Therefore, the 50% inhibition of the liposomal binding was achieved with Fbg of which concentration is 25-fold excess of H12.

It is known that several peptides derived from amino acid sequence in Fbg, including the H12 peptide, competitively inhibit the binding of Fbg to platelets (Timmons et al., 1984; Gartner and Bennett, 1985; Plow et al., 1985). However, the affinity of these peptides for platelets is known to be less than one-tenth of that of native fibrinogen (Ruggeri et al., 1986). Therefore, it may be concluded that liposomalization of H12, which enabled multivalent and cooperative binding to the target molecules with high density of ligands, gave liposomes the binding ability to GPIIb/IIIa superior to Fbg overwhelmingly without losing the specificity of H12 to GPIIb/IIIa.

In the experiment on the ability of H12-(ADP)Lipo to bind to platelets in the presence of Fbg (Fig. 4), the concentrations of Fbg, H12-(ADP)Lipo and H12 peptide on the surface of liposome were about 3.6×10^{12} molecules/μL (6 μM), 4.0×10^{8} particles/μL (final concentration, 0.5 mg/mL as lipids) and 1.2×10^{12} molecules/μL (2 μM), respectively. The number of particles of H12-(ADP)Lipo was calculated by using the particle size and the data of each compositional lipid of the liposomes with the CAD device. Considering the values of the above-mentioned components, the number of H12 peptide molecules present on the surface of a single H12-(ADP)Lipo is calculated to be about 1400 molecules. In the reaction liquid, the number of Fbg molecules was approximately 9000-fold and 6.2-fold over the number of H12-(ADP)Lipo and H12 peptide chains, respectively, on the surface of the liposomes. These numbers mean that H12 molecules on the H12-(ADP)Lipo show far stronger affinity for platelets than does Fbg due to the cooperative effect by liposomalization and can overcome the influence of a large amount of Fbg in the blood.

5. Conclusions

GPIIb/IIIa-specific H12 peptides modified on the liposomal surface cooperatively and strongly bind to GPIIb/IIIa on the surface of activated platelets: the multivalent binding between H12 peptides and GPIIb/IIIa strengthened the binding of the liposomes to activated platelets. This strong binding could overcome the influence of the physiological concentration Fbg; therefore, H12-(ADP)Lipo may be considered as a candidate for a hemostat.

Acknowledgments

The authors thank Mr. T. Iwao, Mr. Y. Nawa, Dr. S. Okamura, Ms. K. Eto, Mr. S. Katsuno, Ms. H. Maruyama, and Ms. M. Arai for their support of this work. They also thank Dr. H. Saito and Ms. Y. Suzuki for technical support in analyzing characteristics of the liposomes.

References

Agam, G., Livine, A.A., 1992. Erythrocytes with covalently bound fibrinogen as a cellular replacement for the treatment of thrombocytopenia. Eur. J. Clin. Invest. 22, 105–112.

Andrieux, A., Hudry-Clergeon, G., Ryckewaert, J.J., Chapel, A., Ginsberg, M.H., Plow, E.F., Marguerie, G., 1989. Amino acid sequences in fibrinogen mediating its interaction with its platelet receptor, GPIIb/IIIa. J. Biol. Chem. 264, 65–9258.

Blajchman, M.A., 2003. Substitutes and alternatives to platelet transfusions in thrombocytopenic patients. J. Thromb. Haemost. 1, 1637–1641.

Casals, E., Verdaguer, A., Tonda, R., Galan, A., Escolar, G., Estelrich, J., 2003. Atomic force microscopy of liposomes bearing fibrinogen. Bioconjug. Chem. 14, 593–600.

Coller, B.S., Springer, K.T., Beer, J.H., Mohandas, N., Scudder, L.E., Norton, K.J., West, S.M., 1992. Thromboerythrocytes. In vitro studies of a potential autologous, semi-artificial alternative to platelet transfusion. J. Clin. Invest. 89, 546–555.

Du, X., Plow, E.F., Frelinger III, A.L., O'Toole, T.E., Loftus, J.C., Ginsbeg, M.H., 1991. Ligands "activate" integrin αIIbβ3 (platelet GPIIb-IIIa). Cell 65, 409–416.

Gartner, T.K., Bennett, J.S., 1985. The tetrapeptide analogue of the cell attachment site of fibronectin inhibits platelet aggregation and fibrinogen binding to activated platelets. J. Biol. Chem. 260, 11891–11894.

Graham, S.S., Gonchoroff, N.J., Miller, J.L., 2001. Infusible platelet membranes retain partial functionality of the platelet GPIb/IX/V receptor complex. Am. J. Clin. Phathol. 115, 144–147.

Halle, M., Berg, A., Keul, J., Baumstark, M.W., 1996. Association between serum fibrinogen concentrations and HDL and LDL subfraction phenotypes in healthy men. Arterioscler. Thromb. Vasc. Biol. 16, 144–148.

Kloczewiak, M., Timmons, S., Lukas, T.J., Hawiger, J., 1984. Platel receptor recognition site on human fibrinogen. Synthesis and structure-function relationship of peptides corresponding to the carboxy-terminal segment of the gamma chain. Biochem. 23, 1767–1774.

Kuwahara, M., Sugimoto, M., Tsuji, S., Matsui, H., Mizuno, T., Miyata, S., Yoshioka, A., 2002. Platelet shape changes and adhesion under high shear flow. Arterioscler. Thromb. Vasc. Biol. 22, 329–334.

Levi, M., Friedrich, P.W., Middleton, S., De Groot, P.G., Wu, Y.P., Harris, R., Biemond, B.J., Heijien, F.G., Levin, J., Ten Cate, J.W., 1999. Fibrinogen-coated albumin microcapsules reduce bleeding in severely replacement for the treatment of thrombocytopenic rabbits. Nat. Med. 5, 107–111.

Michael, W.M., 1990. Fibrin polymerization and its regulatory role in hemostasis. J. Lab. Clin. Med. 116, 8–17.

Michael, W.M., 1992. The roles of fibrinogen and fibrin in hemostasis and thrombosis. Semin. Hematol. 29, 177–188.

Milton, J.G., Hutton, R.A., Tuddenham, E.G., Frojmovic, M.M., 1985. Platelet size and shape in hereditary giant platelet syndromes on blood smear and in suspension: evidence for two types of abnormalities. J. Lab. Clin. Med. 106, 326–335.

Okamura, Y., Takeoka, S., Teramura, Y., Maruyama, H., Tsuchida, E., Handa, M., Ikeda, Y., 2005a. Hemostatic effects of fibrinogen γ-chain dodecapeptide-conjugated polymerized albumin particles in vitro and in vivo. Transfusion 45, 1221–1228.

Okamura, Y., Maekawa, I., Teramura, Y., Maruyama, H., Handa, M., Ikeda, Y., Takeoka, S., 2005b. Hemostatic effects of phospholipid vesicles carrying fibrinogen γ chain dodecapeptide in vitro and in vivo. Bioconjug. Chem. 16, 1589–1596.

Okamura, Y., Fujie, T., Maruyama, H., Handa, M., Ikeda, Y., Takeoka, S., 2007. Prolonged hemostatic ability of poly(ethylene glycol)-modified polymerized albumin particles carrying fibrinogen γ-chain dodecapeptide. Transfusion 47, 1254–1262.

Okamura, Y., Takeoka, S., Eto, K., Maekawa, I., Murayama, H., Ikeda, Y., Handa, M., 2009. Development of fibrinogen γ-chain peptide-coated, adenosine diphosphate-encapsulated liposomes as a synthetic platelet substitute. J. Thromb. Haemost. 7, 470–477.

Plow, E.F., Pierschbacher, M.D., Ruoslahti, E., Marguerie, G., Ginsberg, M.H., 1985. The effect of Arg-Gly-Asp-containing peptides on fibrinogen and von Willebrand factor binding to platelets. Proc. Natl. Acad. Sci. U.S.A. 82, 8057–8061.

Ruggeri, Z.M., Houghten, R.A., Russell, S.R., Zimmerman, T.S., 1986. Inhibition of platelet function with synthetic peptides designed to be high-affinity antagonists of fibrinogen binding to platelets. Proc. Natl. Acad. Sci. U.S.A. 83, 5708–5712.

Ruoslahti, E., 1996. RGD and other recognition sequences for integrins. Annu. Rev. Cell Dev. Biol. 12, 697–715.

Rybak, M., Renzulli, L.A., 1993. A liposome based platelet substitutes, the plateletsome, with hemostatic efficacy. Biomater. Artif. Cells Immobil. Biotechnol. 21, 108–118.

Takagi, J., Petre, B.M., Walz, T., Springer, T.A., 2002. Global conformational rearrangements in integrin extracellular domains in outside-in and inside-out signaling. Cell 110, 599–611.

Timmons, S., Kloczewiak, M., Hawiger, J., 1984. ADP-dependent common receptor mechanism for binding of von Willebrand factor and fibrinogen to human platelets. Proc. Natl. Acad. Sci. U.S.A. 81, 4935–4939.

Drug Metabolism Reviews, 2011; 43(3): 362–373

ISSN 0360-2532 print/ISSN 1097-9883 online
DOI: 10.3109/03602532.2011.558094

informa
healthcare

REVIEW ARTICLE

Pharmacokinetic properties of hemoglobin vesicles as a substitute for red blood cells

Kazuaki Taguchi[1], Toru Maruyama[1,2], and Masaki Otagiri[1,3]

[1]Department of Biopharmaceutics, Kumamoto University, Kumamoto, Japan, [2]Center for Clinical Pharmaceutical Sciences, Graduate School of Pharmaceutical Sciences, Kumamoto University, Kumamoto, Japan, and [3]Faculty of Pharmaceutical Sciences, Sojo University, Kumamoto, Japan

Abstract

The development of artificial oxygen carriers has attracted considerable recent interest because of the increasing cost of collecting and processing blood, public concerns about the safety of blood products, complications from blood transfusions, military requirements for increased volumes of blood during military conflicts, and a decrease in the number of new donors. To overcome these problems, perfluorocarbon-based oxygen carriers as well as acellular- and cellular-type, hemoglobin-based oxygen carriers have been developed for use as artificial oxygen carriers. Despite their extensive evaluation, including formulation and pharmacology, they have not been extensively used in clinical settings. One of the reasons for this is that their pharmacokinetics have not been well characterized. Artificial oxygen carriers require not only an acceptable level of physicochemical activity, but also clinical efficacy, as reflected by their retention in the circulation, and the absence of measurable accumulation in the body, if unexpected adverse effects are to be avoided. In this review, the pharmacokinetic properties of artificial oxygen carriers are discussed, with a focus on recent developments of our research related to the pharmacokinetic properties a cellular type of hemoglobin-based oxygen carrier.

Keywords: Artificial oxygen carrier, disposition, liposome, mononuclear phagocyte system, hemorrhagic shock, hepatic chronic cirrhosis, accelerated blood clearance phenomenon

Introduction

In modern medical care, there is now little doubt that the transfusion of red blood cells (RBCs) is the gold standard for treatment of patients with massive hemorrhages and is currently in widespread use. Nevertheless, the potential for mismatching exists and infections by unrecognized pathogens, hepatitis, HIV, or West Nile virus, etc., are always a possibility. In addition, ensuring a steady supply of RBCs at a time of a disaster and during military conflicts could be difficult, because the lifetime of donated RBCs is limited to a short period. Further, a decrease in donors and an increase in recipients in some developed countries is also a problem. To overcome these problems, various artificial oxygen carriers have been under development worldwide. They can be divided into three major classes of materials, as follows: perfluorocarbon-based oxygen carriers, acellular-type, hemoglobin-based oxygen carriers (HBOCs), and cellular-type HBOCs (Figure 1). Despite the many efforts to develop artificial oxygen carriers during the past several decades, some of them were, unfortunately, rejected for use as the result of preclinical and clinical trials. It is noteworthy that perfluorocarbon-based oxygen carriers and acellular-type HBOCs were excluded as possible candidates for artificial oxygen carriers, even though they proceeded to the stage of clinical trials.

One of the reasons that induced these adverse effects was due to the insufficient characterization of pharmacokinetics of these artificial oxygen carriers under various situations. The desirable features of artificial oxygen carriers as a substitute for RBCs is not only a long retention in the circulation to sustain its pharmacological effects, but also no bioaccumulation, which could lead to adverse effects. Unlike other drugs, because the dosage volume of

Address for Correspondence: Masaki Otagiri, Department of Biopharmaceutics, Graduate School of Pharmaceutical Sciences, Kumamoto University, 5-1 Oe-honmachi, Kumamoto 862-0973, Japan; Fax: +81-96-362-7690; E-mail: otagirim@gpo.kumamoto-u.ac.jp

(Received 05 October 2010; revised 22 January 2011; accepted 24 January 2011)

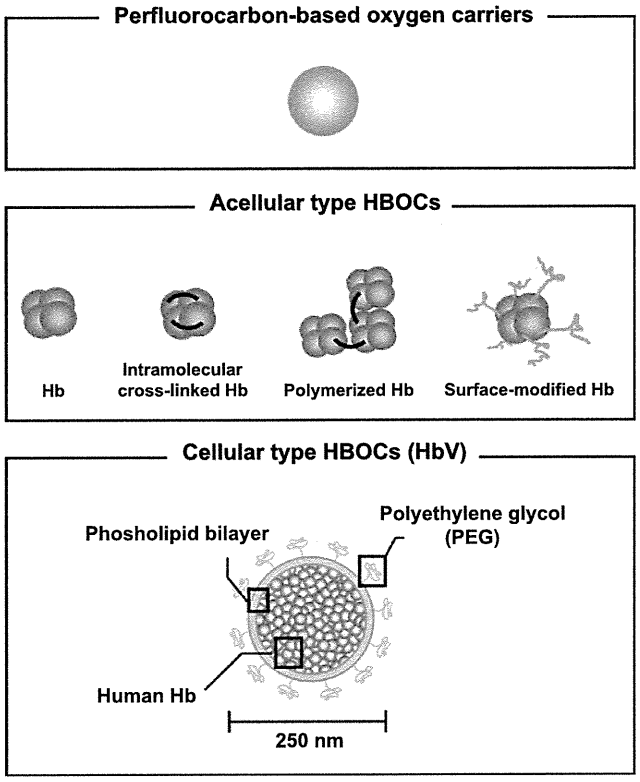

Figure 1. Schematic representation of perfluorocarbon-based oxygen carriers, acellular-type hemoglobin-based oxygen carriers (HBOCs), and cellular-type HBOCs (HbV). In the case of HbV, the surface is modified with polyethylene glycol (PEG) chains, and one HbV particle contains approximately 30,000 human Hb molecules obtained from outdated donated blood. The encapsulated Hb contains pyridoxal 5′-phosphate as an allosteric effector to regulate P_{50} to 25–28 torr. The lipid bilayer was comprised of a mixture of DPPC, cholesterol, and DHSG at a molar ratio of 5:5:1, and DSPE-PEG_{5000} (0.3 mol%). The average particle diameter was regulated to approximately 250 nm.

an artificial oxygen carrier as an RBC substitute is more than a hundred times higher than that of other drugs, detailed information regarding the fate of an artificial oxygen carrier, including its constituent components, is needed, in order to predict unexpected adverse effects.

In this review, the pharmacokinetic properties of artificial oxygen carriers are discussed, with a focus on hemoglobin vesicles (HbVs), in which, among the current artificial oxygen carriers, its pharmacokinetic properties have been extensively characterized.

Perfluorocarbon-based oxygen carriers

The perfluorocarbon-based oxygen carriers are characterized by a high gas-dissolving capacity, low viscosity, and chemical and biological inertness (Spahn and Kocian, 2003). They are molecules that are constructed from cyclic or straight-chain hydrocarbons, in which the hydrogen atoms are replaced by halogens, and are virtually immiscible with water and, therefore, must be emulsified prior to their use in intravenous applications (Pape and Habler, 2007). When perfluorocarbon emulsion droplets are injected into an organism, they are rapidly taken up and slowly broken down by the mononuclear phagocyte system (MPS). After being degraded, the emulsion droplets are again taken up by the blood and transported to the lungs, where any unaltered molecules are excreted via exhalation (Spahn and Kocian, 2003; Jahr et al., 2007; Pape and Habler, 2007). However, perfluorocarbon-based oxygen carriers induced chronic pneumonitis due to their inefficient excretion from the body and their accumulation in the lung, a condition that persists for more than 1 year (Nose, 2004) (Table 1).

Acellular-type HBOCs

The stroma-free hemoglobin (Hb) was developed for use as artificial oxygen carriers, but their systemic half-lives were too short (~0.5–1.5 hours) for them to effectively function as an optimal oxygen carrier (Savitsky et al., 1978). In addition, the Hb tetramers dissociate into their component αβ dimers, which are then eliminated by the kidneys, and induce renal toxicity (Creteur and Vincent, 2003). In an attempt to increase their systemic half-life and stability, the following three groups of chemically modified acellular-type HBOCs were developed: surface-modified Hb (Smani, 2008), intramolecularly cross-linked Hb (Chen et al., 2009), and polymerized Hb (Jahr et al., 2008) (Figure 1). These acellular HBOCs have improved systemic half-lives, in the range of 18–24 hours, and show decreased renal failure (Stowell, 2005) (Table 1). The polymerized bovine-derived Hb has been approved for limited use in South Africa (Lok, 2001). However, it was recently reported that the use of some acellular-type HBOCs leads to the development of myocardial lesions, as the result of decreasing nitric-oxide levels 24–48 hours after a single toploud infusion (Burhop et al., 2004), leading to an increase in mortality rates in humans (Natanson et al., 2008).

Hemoglobin vesicles

The hemoglobin vesicle (HbV) is a cellular-type HBOC that contains polyethylene glycol (PEG), in which phospholipid vesicles encapsulating highly concentrated human Hb are imbedded (Sakai et al., 2008) (Figure 1). The cellular structure of HbV (particle diameter: approximately 250 nm) most closely mimics the characteristics of a natural RBC, such as the cell-membrane function, which physically prevents the direct contact of Hb with the components of blood and the vasculature during its circulation. The characteristics of HbV are superior to donated RBCs in the following ways: the absence of viral contamination (Sakai et al., 1993; Abe et al., 2001), a long-term storage period of over 2 years at room temperature, and no blood-type antigens (Sakai et al., 2000; Sou et al., 2000) (Table 2). In addition, HbVs have the ability to transport oxygen equivalent to RBCs and also show improved survival in hemorrhagic shock animal models (Sakai et al., 2004b; Terajima et al., 2006; Sakai et al., 2009). Further, HbVs can control the release of oxygen by

adjusting the amount of allosteric effector and regulate rheological properties (e.g., viscosity and colloid osmotic pressure) to added human serum albumin (Sakai and Tsuchida, 2007). Therefore, HbV has attracted considerable attention as a possible new artificial oxygen carrier and has considerable promise for use in clinical settings.

We recently characterized the pharmacokinetic properties of HbV to clarify its efficacy and safety under conditions that mimic a clinical setting, as follows:

1. HbV was constructed from multiple components, including Hb, lipids, and iron from Hb. These components have potential risks for inducing harmful effects, when they accumulate at excessive levels in the body.
2. HbV is classified as a liposome preparation. It was previously reported that the pharmacokinetics of liposome-encapsulated amphotericin B differ between normal individuals and patients (Walsh et al., 1998; Bekersky et al., 2001).
3. The surface of HbV was modified by PEG to enhance the half-life in circulation and storage. It was recently reported that repeated injection of PEGylated liposomes influenced the pharmacokinetics of the second injected liposome (Dams et al., 2000; Ishida et al., 2003a).

Table 1. Pharmacokinetic properties of some artificial oxygen carriers.

	Perfluorocarbon-based oxygen carriers	Acellular-type HBOCs	Cellular-type HBOCs
Distribution	Liver, spleen	Liver	Liver, spleen
Metabolism	MPS	MPS	MPS
Excretion	Air	—	Internal Hb; urine outer membrane; feces
Half-life	~10 hours (rat)	~24 hours (rat)	30~40 hours (rat)
Existence in tissues	~1 year	—	~14 days

HBOCs, hemoglobin-based oxygen carriers; MPS, mononuclear phagocyte system.

Table 2. Physicochemical characteristics of HbV.

Parameter	
Particle diameter	ca. 250 nm
P_{50}	25–28 torr
Hb concentration	10 g/dL
MetHb	<3%
Colloid osmotic pressure	0 Torr
Intracellular Hb concentration	ca. 35 g/dL
Lipid composition[a]	DPPC/cholesterol/DHSG/DSPE-PEG_{5000}
Stability for storage at room temperature	Over 2 years, purged with N_2

[a]DPPC, 1,2-dipalmitoyl-*sn*-glycero-3-phosphatidylcholine; DHSG, 1,5-bis-*O*-hexadecyl-*N*-succinyl-L-glutamate; DSPE-PEG_{5000}, 1,2-distearoyl-*sn*-glycero-3-phosphatidyl-ethanolamine-*N*-PEG.

For these reasons, it becomes necessary to clarify the pharmacokinetic properties of HbV in various animal models and under conditions of repeated injection, if RBCs are to be used as a substitute in the future. For this purpose, 1) the disposition of HbVs was examined using isotope tracer techniques. In these experiments, ^{125}I-HbV, enclosed in HbVs, was radiolabeled with ^{125}I, and the lipid component vesicles of HbVs was radiolabeled with ^{3}H; 2) a pharmacokinetic study of HbVs in a rat model of hemorrhagic shock and hepatic chronic cirrhosis; 3) the repeated injection in normal and the hemorrhagic shock rat model; and 4) animal scale-up using an allometric equation, were conducted.

Some highlights of recent developments of our research related to the pharmacokinetic properties of HbV are discussed below.

The prior pharmacokinetic characteristics of HbV to stroma-free Hb

Two requirements need to be satisfied if HbV is to be accepted for use as an artificial oxygen carrier. For clinical applications, HbVs must have not only an acceptable physicochemical activity, but also must be safe for use in the clinic. In the latter case, the supply of oxygen tissues is one of the most important factors in sustaining the clinical effect of HbVs (Takaori, 2005). To fulfill these requirements, a prolonged half-life is a required property for HbVs.

We recently demonstrated that the half-life of HbV in mice was 30 times higher than that of stroma-free Hb at a dose rate of 1 mg Hb/kg (Table 3). Moreover, a dose-dependent study clearly showed that the plasma concentration curve and half-life of HbV in mice and rats increased with increasing doses of HbV (Figure 2, half-life; rats: 8.8±0.7, 11.5±0.3, and 30.6±4.0 hours at doses of 10, 200, and 1,400 mg Hb/kg, respectively; mice: 3.1±3.1, 3.6±1.3, 7.2±3.1, and 18.8±1.3 hours at doses of 1, 10, 200, and 1,400 mg Hb/kg, respectively) (Taguchi et al., 2009b).

These superior pharmacokinetic characteristic of HbV, compared to stroma-free Hb, could reflect their physicochemical differences, such as particle diameter, the absence or presence of a membrane structure, and PEG modification. In physiological conditions, free Hb that is released from ruptured RBC is rapidly bound to

Table 3. Pharmacokinetic parameters for HbV after the administration of ^{125}I-Hb and ^{125}I-HbV in mice at a dose of 1 mg Hb/kg.

	^{125}I-Hb	^{125}I-HbV	*p*
$t_{1/2}$ (hr)	0.1±0.1	3.1±1.0	<0.01
AUC (hr*% of dose/mL)	7.9±3.9	29.4±9.2	<0.001
CL (mL/hr)	12.7±2.1	3.4±0.1	<0.001
V (mL)	2.6±0.3	2.3±0.1	N.S.

$t_{1/2}$, half-life; AUC, are under the plasma-concentration versus time curve; CL, clearance; V, distributed volume; N.S., not significant.

haptoglobin (Hp), which promotes CD163 recognition in the liver (Kristiansen et al., 2001). When the Hb concentration exceeds the Hp-binding capacity, unbound Hb is removed by filtration through the kidney. Therefore, the reduction in HbV distribution in the liver and kidney could be due to the encapsulation of Hb by liposomes because this might not only suppress the binding of internal Hb to Hp, but also inhibit renal glomerular filtration. In fact, it was observed that the distribution of HbV in the liver and kidney was suppressed, compared with that of stroma-free Hb (Taguchi et al., 2009b). Moreover, the membrane surface modification by PEG also contributed to the increased half-life of HbV. In general, it is well-known that liposomes are scavenged and degraded by the MPS, such as Kupffer cells or macrophages in the spleen (Kiwada et al., 1998). PEGylation is a useful method for suppressing the capture of MPS, and the majority of the recently developed liposome formulations are modified with PEG (Noble et al., 2006; Sou et al., 2007; Okamura et al., 2009). Therefore, the modification of HbV with PEGylation is important to not only stabilize for a long-time storage, but also to maintain the good retention in the circulation. These balanced physicochemical activities result in a longer retention in the circulation, compared to stroma-free Hb and acellular-type HBOCs (Goins et al., 1995; Chang et al., 2003; Lee et al., 2006).

The disposition of HbV components

In clinical situations as a substitute of RBCs, massive amounts of HbV are typically given to patients. As a result, its associated components, including Hb, lipids from Hb, could result in undesirable consequences in the systemic circulation and organs during its metabolism and disposition. Such an extraordinary load of HbV components could result in the accumulation of components in the blood or organs, and has the potential to cause a variety of adverse effects, as follows: 1) high levels of lipid components, especially cholesterol, in the bloodstream, which are risk factors for kidney disease, arterial sclerosis, and hyperlipidemia (Grone and Grone, 2008); 2) Hb induces renal toxicity by dissociation of the tetramic Hb subunits into two dimers (Parry, 1988); and 3) free iron can trigger tissue damage induced by the Fenton reaction, which is mediated by heme (iron) (Balla et al., 2005). Therefore, it becomes necessary to clarify whether HbV and its components have favorable metabolic and excretion profiles. In order to investigate the disposition of each HbV component, Hb, enclosed in HbV, was radiolabeled with ^{125}I (^{125}I-HbV) or cholesterol, in the lipid component vesicles of HbV, was radiolabeled with ^{3}H (^{3}H-HbV).

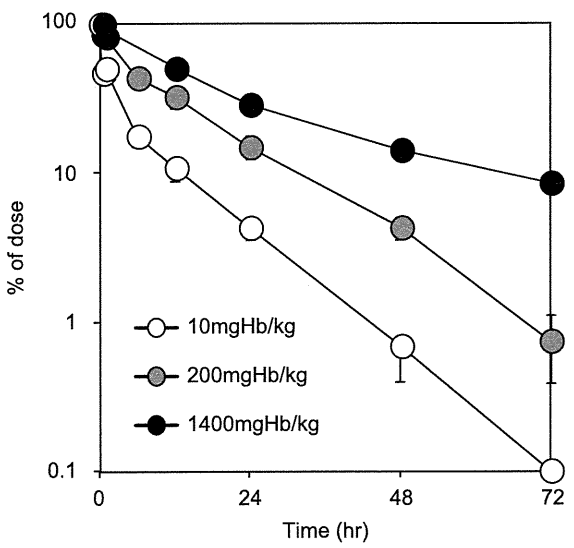

Figure 2. Dose-dependent plasma concentration curve of ^{125}I-HbV after administration of ^{125}I-HbV in rats. All rats received a single injection of ^{125}I-HbV at a dose of 10 (open squares), 200 (gray circles), and 1,400 mg Hb/kg (closed circles) containing 5% rHSA. At each time point (0.05, 0.5, 1, 6, 12, 24, 48, and 72 hours) after the ^{125}I-HbV injection, blood samples were collected from the tail vein, and a plasma sample was obtained. Each point represents the mean ± SD (n=3–5).

In the blood circulation, HbV typically maintains an intact structure for periods of up to 72 hours after injection, because similar plasma concentration curves for ^{125}I-HbV were observed for ^{3}H-HbV in rats (Figure 3A), and the pharmacokinetic parameters were also consistent between them (half-life: 30.6 ± 4.0, 30.9 ± 4.7 hours; clearance in plasma: 0.46 ± 0.04, 0.41 ± 0.02 mL/h, for ^{125}I- and ^{3}H-HbV, respectively). Moreover, ^{125}I-HbV and ^{3}H-HbV were mainly distributed in the liver and spleen (Figure 3B). Because HbV possesses a liposome structure, it would be predicted that it would be captured by the MPS in the liver and spleen (Kiwada et al., 1998). In fact, a previous *in vitro* study clearly demonstrated that HbV was specifically taken up and degraded in RAW 264.7 cells, which has been used as an alternative to Kupffer cells, but this was not the case for parenchymal and endothelial cells (Taguchi et al., 2009b). In addition, the uptake clearance (CL_{uptake}) in the liver and spleen were also similar between the two labeled preparations (liver: 1,141 ± 142, 1,098 ± 123; spleen: 619 ± 40, 518 ± 89 μL/h, for ^{125}I-HbV and ^{3}H-HbV, respectively). However, ^{125}I was more rapidly eliminated from each organ, and the activity essentially disappeared within 7 days. On the other hand, the elimination of radioactive ^{3}H was delayed, compared to that of ^{125}I, but nearly disappeared after 14 days. These data indicate that HbV is mainly distributed to the liver and spleen in the form of intact HbV, and that it was degraded by the MPS. In order to identify the excretion pathway of HbV, the levels of radioactivity of ^{125}I and ^{3}H in the urine and feces were measured. The radioactive ^{125}I was excreted mainly in the urine, whereas the majority of the ^{3}H was excreted in the feces. Based on the above findings, the disposition of HbV and its components, after circulating in the form of stable HbV, are distributed to the liver and spleen, where they are degraded by the MPS. Finally, the enclosed Hb and outer lipid components were mainly eliminated to the urine and feces, respectively, in the same manner as endogeneous substances (Figure 4). Similar results were also reported in mice and rabbits (Sou et al.,

2005; Taguchi et al., 2009b); these results indicate that HbV and its components have favorable metabolic and excretion profiles in mammalian species. In addition, the plasma concentration curve for heme (iron) derived from HbV was similar to that for ^{125}I-HbV and ^{3}H-HbV in mice (Taguchi et al., 2009b). Moreover, no significant differences in the ratio of the mercapt- (i.e., nonoxidized form) to the nonmercapt-form (i.e., oxidized form) of rat serum albumin, which serves as a marker of oxidative stress in the circulation system (Kadowaki et al., 2007; Shimoishi et al., 2007), were found between HbV and the saline administration groups for periods of up to 7 days after administration. These results suggest that excess free heme (iron) derived from HbV is not released in the plasma. However, the issue of the disposition of several HbV components, including PEG and phospholipid, was not clarified. It is also possible that these components in HbV are also metabolized and excreted in the same manner as endogenous substances, but further study will be needed to demonstrate this fact.

Pharmacokinetic properties of HbV under conditions of hemorrhagic shock

It is well known that clinical conditions can have an effect on the pharmacokinetics of numerous drugs (Abernethy et al., 1981; Turck et al., 1996). For example, it has demonstrated that the pharmacokinetics of liposome-encapsulated amphotericin B differ between normal individuals and patients in a clinical trial stage (Walsh et al., 1998; Bekersky et al., 2001). Consequently, it is possible that the pharmacokinetics of HbV would be also altered in the situation of a massive hemorrhage caused by injury, accidental blood loss, or a major surgery. To clarify this, we investigated the changes in HbV pharmacokinetics using a rat model of hemorrhagic shock induced by massive hemorrhage.

As shown in Figure 5, the retention of HbV in plasma under this condition was shorter, and the half-life of HbV was reduced significantly—by 0.66-fold—compared with the half-life of HbV in normal rats (30.6±4.0, 18.1±3.7 hours, for normal and hemorrhagic shock, respectively). At a glance, this appears to not be a desirable situation for the therapeutic use of HbV, because an important determinant of HbV efficacy is a long retention in the blood circulation. However, the distribution volume of the central compartment of HbV (V_1) was identical between normal and hemorrhagic shock rats, whereas the distribution volume of the peripheral compartment (V_2) in hemorrhagic shock rats was nearly 2-fold greater than that of normal rats (Figure 5, insert). Moreover, the time-course tissue distribution of HbV in the hemorrhagic shock rats was greater than normal rats. These findings indicate that the shorter half-life in hemorrhagic shock rats appears to be the result in an apparent reduction in HbV in the arteriovenous circulation. If this enhanced tissue distribution of HbV might be derived by an increased scavenging of HbV by the MPS, such as by Kupffer cells, red pulp zone splenocytes, and mesangial cells (Sakai et al., 2004a), it would not be expected to show significant pharmacological efficacy as an oxygen carrier, because HbV must maintain an intact structure to maintain its oxygen-carrying capacity. However, the pharmacological effect in the hemorrhagic shock model animal was significantly increased by the HbV treatment, similar to that for an RBC treatment (Sakai et al., 2004b; Terajima et al., 2006; Sakai et al., 2009). In addition, the amount of excretion into the urine, which is the major elimination pathway, did not differ between normal and hemorrhagic shock rats in our pharmacokinetic study. Therefore, HbV appears to be transferred from the arteriovenous blood to organ capillary beds as an intact structure, and is not excessively captured and metabolized by the MPS. These findings support the conclusion

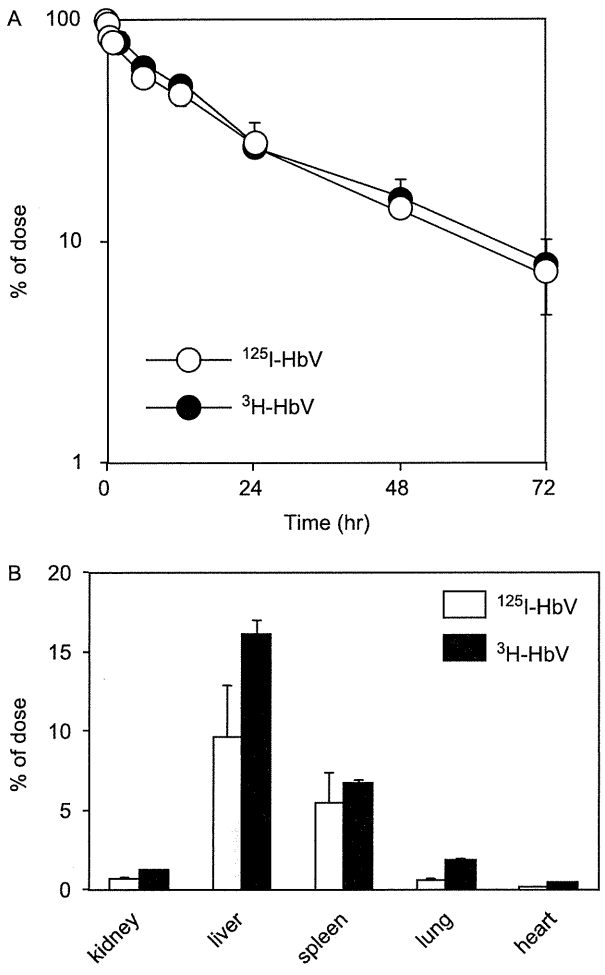

Figure 3. (**A**) Time course for the plasma level of ^{125}I-HbV (open circles) and ^{3}H-HbV (filled circles) after administration to rats. SD rats received a single injection of ^{125}I-HbV or ^{3}H-HbV to the tail vain at a dose of 1,400 mg Hb /kg. Blood was collected from the tail vein under ether anesthesia, and a plasma sample was obtained. Each point represents the mean ± SD (n=5). (**B**) Tissue distributions of ^{125}I-HbV (open bars) and ^{3}H-HbV (filled bars) at 24 hours after administration to mice. SD rats received a single injection of ^{125}I-HbV or ^{3}H-HbV from the tail vain at a dose of 1,400 mg Hb/kg. At 24 hours after injection, each organ was collected. Each bar represents the mean ± SD (n=5).